



A Comprehensive Toolkit for Quick and Easy Visualization of Marker Proteins, Protein–Protein Interactions and Cell Morphology in *Marchantia polymorpha*

Jens Westermann^{†‡}, Eva Koebke[‡], Roswitha Lentz, Martin Hülskamp and Aurélien Boisson-Dernier^{*}

Institute for Plant Sciences, Faculty of Mathematics and Natural Sciences, University of Cologne, Cologne, Germany

OPEN ACCESS

Edited by:

Elison B. Blancaflor,
Noble Research Institute, LLC,
United States

Reviewed by:

Mario Alberto Arteaga-Vazquez,
Universidad Veracruzana, Mexico
Satoshi Naramoto,
Hokkaido University, Japan

*Correspondence:

Aurélien Boisson-Dernier
aboisson@uni-koeln.de

† Present address:

Jens Westermann,
Department of Biology, Institute
of Molecular Plant Biology, Swiss
Federal Institute of Technology
in Zurich, Zurich, Switzerland

‡ These authors have contributed
equally to this work

Specialty section:

This article was submitted to
Plant Cell Biology,
a section of the journal
Frontiers in Plant Science

Received: 03 June 2020

Accepted: 22 September 2020

Published: 15 October 2020

Citation:

Westermann J, Koebke E,
Lentz R, Hülskamp M and
Boisson-Dernier A (2020) A
Comprehensive Toolkit for Quick
and Easy Visualization of Marker
Proteins, Protein–Protein Interactions
and Cell Morphology in *Marchantia*
polymorpha.
Front. Plant Sci. 11:569194.
doi: 10.3389/fpls.2020.569194

Even though stable genomic transformation of sporelings and thalli of *Marchantia polymorpha* is straightforward and efficient, numerous problems can arise during critical phases of the process such as efficient spore production, poor selection capacity of antibiotics or low transformation efficiency. It is therefore also desirable to establish quick methods not relying on stable transgenics to analyze the localization, interactions and functions of proteins of interest. The introduction of foreign DNA into living cells via biolistic mechanisms has been first reported roughly 30 years ago and has been commonly exploited in established plant model species such as *Arabidopsis thaliana* or *Nicotiana benthamiana*. Here, we report the fast and reliable transient biolistic transformation of *Marchantia* thallus epidermal cells using fluorescent protein fusions. We present a catalog of fluorescent markers which can be readily used for tagging of a variety of subcellular compartments. Moreover, we report the functionality of the bimolecular fluorescence complementation (BiFC) in *M. polymorpha* with the example of the p-body markers MpDCP1/2. Finally, we provide standard staining procedures for live cell imaging in *M. polymorpha*, applicable to visualize cell boundaries or cellular structures, to complement or support protein localizations and to understand how results gained by transient transformations can be embedded in cell architecture and dynamics. Taken together, we offer a set of easy and quick tools for experiments that aim at understanding subcellular localization, protein–protein interactions and thus functions of proteins of interest in the emerging early diverging land plant model *M. polymorpha*.

Keywords: *Marchantia polymorpha*, biolistic bombardment, staining, cell biology, cellular localization, BiFC, FERONIA (FER), Dcp1/Dcp2

INTRODUCTION

In the last decade, the liverwort *Marchantia polymorpha* has emerged as a powerful model system to study early land plant evolution due to its early evolutionary divergence in the land plant phylogenetic tree (Shaw et al., 2011; Harrison, 2017; Morris et al., 2018). Research deploying *M. polymorpha* has led to a series of insightful studies on the functional evolution of abscisic acid

(ABA, Lind et al., 2015; Eklund et al., 2018) and jasmonic acid (JA) signaling mechanisms (Monte et al., 2018, 2019; Peñuelas et al., 2019), plant immunity (Carella et al., 2019; Gimenez-Ibanez et al., 2019), reproductive and vegetative development (Flores-Sandoval et al., 2015; Proust et al., 2016; Jones and Dolan, 2017; Rövekamp et al., 2016; Otani et al., 2018; Westermann et al., 2019; Thamm et al., 2020) and cell division (Buschmann et al., 2016). It offers the advantage of genetic and morphological simplicity in combination with its dominant haploid vegetative life phase, allowing for fast generation of knockout mutants and subsequent phenotypic analyses, irrespectively of time-consuming homozygous mutant generation (Ishizaki et al., 2015b). Concomitantly, a plethora of molecular genetic tools was developed that include stable transformation of developing spores (Ishizaki et al., 2008) and regenerating thallus fragments (Kubota et al., 2013), the suitability for genome editing via homologous recombination (Ishizaki et al., 2013) and CRISPR/Cas9 (Sugano et al., 2014; Sugano and Nishiyama, 2018), the cultivation in axenic conditions and on soil and controlled crossing (Ishizaki et al., 2015b). Finally, the community benefits now from the availability of the fully sequenced and annotated *M. polymorpha* genome (Bowman et al., 2017).

Plant genetics and cell biological approaches generally rely on the efficient visualization of intracellular features, including protein localization and organelle architecture or dynamics. In this regard, the process of transient and stable transformation of plant cells is a powerful and commonly used technique in molecular genetics and cell biology to study protein dynamics, as well as genetic and physical (i.e. protein) interaction. It thus aids the elucidation of fundamental biological questions at the (sub)cellular scale. While the performance of stable biolistic transformation of immature thalli and spores has been reported before (Takenaka et al., 2000; Chiyoda et al., 2008, 2014; Sauret-Güeto et al., 2020), we describe here the transient biolistic transformation of *Marchantia* thallus epidermal cells, a technique to study protein localization in living cells that has commonly been used in other plant systems for 30 years (Sanford, 1990; Rasmussen et al., 1994; Ueki et al., 2009). Importantly, we provide a comprehensive list of protein marker constructs that allows quick visualization of a variety of subcellular compartments within 24 h and the possibility for live-imaging. The marker list comprises constructs for visualization of the nucleus, cytoplasm, plasma membrane, actin filaments, endosomes, peroxisomes, the Golgi apparatus and processing bodies (**Supplementary Table S1**).

Genetic interaction studies often rely on assessment of physical protein interactions to elucidate intracellular signaling mechanisms. Therefore, the bimolecular fluorescence complementation technique (BiFC; Hu et al., 2002; Walter et al., 2004) represents a time-efficient method to test for potentially interacting proteins *in vivo*. Hence, we also provide here evidence for the functionality of BiFC in *Marchantia* epidermal cells.

In addition to transient expression, dye-based staining procedures represent a fast and reliable method to (co)visualize subcellular compartment architecture and dynamics. Therefore, we here provide a series of staining protocols for different organelles, both for *Marchantia* thallus epidermal cells and

rhizoids and compare functionality regarding standard protocols used for the seed plant model *Arabidopsis thaliana*.

Moreover, we compiled a list of available *Marchantia* resources, methods, tools and databases (**Table 1**) that altogether will be useful for the young and growing research community that uses *M. polymorpha* as a model system complementing and further supporting its genetic/cell biological/biochemical approaches.

MATERIALS AND METHODS

In order to perform the protocols described below, we recommend having the following materials and equipment available (**Table 2**).

Methods

Plant Material and Growth Conditions

The widely used *Marchantia polymorpha* Tak-1 (MpTak-1) ecotype was cultivated via propagation of vegetative propagules (gemmae) on solid Johnson's medium (Ishizaki et al., 2008) supplemented with 0.8% micro agar under axenic conditions. Cultivation petri dishes were sealed using Micropore tape to ensure gas exchange while preventing microbe contamination. Gemmae were grown under long day condition (16 h light/8 h darkness cycle) and white light irradiation ($60 \mu\text{mol m}^{-2} \text{s}^{-1}$) at 21°C and 60% humidity. After 2.5–3 weeks, a few thallus fragments of approximately 0.5–1 cm² were transferred onto a small petri dish (6–9 cm in diameter) containing fresh solid Johnson's medium on the day of transformation (**Figure 1A**).

The *Arabidopsis thaliana* Col-0 ecotype used for DAPI staining was cultivated on soil and grown under long day conditions at 21°C and $120 \mu\text{mol m}^{-2} \text{s}^{-1}$ light intensity.

Cloning of DNA Constructs

All constructs used in this study are summarized in **Supplementary Table S1**, including their origin, promoter, fluorescent tag and oligonucleotide sequences used for PCR-based amplification of new constructs from *Marchantia* whole-thallus cDNA. The 35S promoter was used for all expression experiments (except for expression of AtSYP32, AtGot1p and LifeAct) to guarantee comparability of subsequent analyses. The coding sequences of interest were cloned into Gateway (GW)-compatible entry vectors, pDONR201 and pDONR207 (Invitrogen), and then remobilized to be integrated in the respective GW destination vectors (**Supplementary Table S1**). The cloning procedure was as described before (Westermann et al., 2019).

DNA Sample Preparation for Biolistic Transformation

For a single shot, 300 ng of vector DNA were mixed with gold, serving as micro-carriers (30 mg/ml, 1 μm , CaCl₂ (2.5 M), spermidine (0.1 M) and ddH₂O under thorough shaking. Subsequently, micro-carriers were washed with 70% EtOH and 100% EtOH. The DNA-coated gold particles were suspended in 100% EtOH and placed onto macro-carriers. The EtOH was allowed to vaporize and the prepared macro-carriers were then used for biolistic transformation.

TABLE 1 | Important Marchantia resources.

Gene and genome databases		
Resource/method	Link	References
Marchantia genome sequence and database	http://marchantia.info/	Bowman et al. (2017)
Marchantia entry on phytozome (including BLAST and genome browser)	https://phytozome.jgi.doe.gov/pz/portal.html#!info?alias=Org_Mpolymorpha	Bowman et al. (2017)
Marchantia chloroplast genome studies		Fukuzawa et al. (1988); Kohchi et al. (1988); Ohyama et al. (1988); Umesono et al. (1988)
MarpoDB: gene-centric database for <i>Marchantia polymorpha</i> genetic parts for purposes of genetic engineering and synthetic biology	http://marpodb.io/query	Delmans et al. (2017)
PlantTFDB: Plant transcription factor database	http://planttfdb.cbi.pku.edu.cn/index.php?sp=Mpo	Jin et al. (2014, 2015, 2017)
Transient and stable genetic modification		
Homologous recombination-mediated genome editing		Ishizaki et al. (2013)
Stable Agrobacterium-mediated thallus transformation		Kubota et al. (2013)
Stable Agrobacterium-mediated sporeling transformation		Ishizaki et al. (2008)
Design of Gateway-compatible vectors for expression in Marchantia		Ishizaki et al. (2015a); Mano et al. (2018)
CRISPR-Cas-based genome editing		Sugano et al. (2014); Sugano and Nishiyama (2018)
CRISPRdirect target search	https://crispr.dbcls.jp/	Naito et al. (2015)
Stable biolistic sporeling/thallus transformation		Chiyoda et al. (2008); Sauret-Güeto et al. (2020)
Comprehensive catalog of fluorescent cell compartment markers		This study
Protein-protein interaction studies via BiFC		This study
Cellular staining techniques		
FM4-64 staining of epidermal cells and rhizoids		Kato et al. (2017) (gemmae cups); this study (whole thallus and rhizoids)
FM1-43 staining of epidermal cells		Minamino et al. (2018)
PI staining of thallus epidermal cells and rhizoids		Fixed cells: Buschmann et al. (2016); Rövekamp et al. (2016) Living cells: Delmans et al. (2017); Jones and Dolan (2017); Thamm et al. (2020); this study
DAPI staining of epidermal cells		Kondou et al. (2019); this study
FDA staining of protoplasts, thallus epidermal cells and rhizoids		Viable protoplasts: Sugawara and Fukukawa (1995); Thallus epidermal cells and rhizoids: This study
Feulgen staining of antheridia and spermatids		Higo et al. (2018)
GUS staining		Takenaka et al. (2000); Higo et al. (2018)
Further resources		
Expressed sequence tags (EST) sequencing		Nagai et al. (1999); Nishiyama et al. (2000)
RNA sequencing of the gametophyte transcriptome		Sharma et al. (2014)
3D imaging using micro-computed tomography and mathematical image-processing method		Furuya et al. (2019)
Guidelines for Marchantia gene nomenclature		Bowman et al. (2015)
Cryo-conservation of Marchantia gemmae		Sauret-Güeto et al. (2020)

Biolistic Transformation Procedure and Efficiency of (Co-)Transformation

Marchantia thallus fragments were placed into a PDS-1000/He Biolistic® Particle Delivery System (Bio-Rad). A vacuum of 25 in Hg vac was applied and the DNA-coated gold particles were shot at 900 psi from a distance of 10 cm. Finally, the bombarded plant material was allowed to recover for 24 h in darkness while remaining in its humid environment, i.e., on the media in the closed petri dish (**Figure 1C**). Biolistic transformation generally yielded $n > 50$ transformed cells per sample shot. A representative example for transformation

efficiency is shown in **Figure 1B**. Moderate to strong expression levels in each individual cell could be observed irrespectively of the protein construct or promoter used (**Figure 1B** and **Supplementary Table S1**). The use of strong promoters such as pro35S, proAtUBQ10 or proMpEF1 α can sometimes lead to overexpression artifacts that may impede drawing secured conclusions. However, yielding a wide range of expression level in the same experimental round and plant sample allows for identification of biologically meaningful protein localization patterns and to distinguish them from unwanted artifacts, such as protein over-accumulation. In order to reliably

assess the potential of transformed constructs as single cell fluorescent markers, we co-bombarded all described vectors with either the nuclear marker AtKRP1 or the plasma membrane markers AtNPSN12 or MpSYP13a fused to fluorescent tags and subsequently created a collection of functional and useful Arabidopsis- and Marchantia-derived fluorescent protein fusions (**Supplementary Table S1**). In order to determine the efficiency of co-transformation, we counted cells expressing both markers in relation to the total number of transformed cells in nine independent co-transformations of protein fusions used in this study. Successful biolistic co-transformation reached on average 74% (see **Supplementary Table S3**).

Staining Procedures

For fluorescein diacetate (FDA) staining, young (2- to 5-day-old) gemmae were placed onto depression slides and covered with an FDA solution (5 mg/L FDA in ddH_2O , diluted from a stock solution of 5 mg/ml FDA in acetone) for 5–10 min. Afterward, samples were rinsed in ddH_2O .

For PI staining, young gemmae were placed onto depression slides and directly covered with a PI solution for 10 min (10 mg/L in ddH_2O). Subsequently, samples were rinsed with ddH_2O .

For FM4-64 staining, young gemmae were mounted onto depression slides in 2 μM FM4-64 diluted in liquid Johnson's growth medium (Ishizaki et al., 2008) and allowed to incubate for 10 min prior to imaging. For FM4-64 and FDA co-staining, gemmae were first stained in a FDA solution and then mounted in a FM4-64 solution, both as described above. Marchantia thallus fragments, transiently transformed with eYFP-MpRAB5 or MpARA6-eYFP, were stained the day after particle bombardment prior to imaging as described above.

For DAPI staining, several methods were used. Experiments were done using 0-, 4-, and 7-day-old gemmae. The DAPI staining solutions were composed of 10–100 mg/L DAPI in either 1xPBS-T (phosphate buffered saline + 0.1% Tween-20) and 5% DMSO or ddH_2O with 0.1 or 1% Tween-20 and 5% DMSO. Different staining incubation times of 10, 30, or 60 min were tested. The staining was tested with and without preceding or subsequent shaking of the samples in 70% EtOH at 80°C. To enhance permeability of membranes, 10 or 50 mg/L digitonin was added to the aforementioned staining solutions. As all attempts for staining living cells failed, the following fixation methods were tested. Gemmae were fixed in a 3:1 EtOH:acetic acid mixture on ice for 1 h, washed three times in 100% EtOH and stained in aforementioned DAPI solutions for 1 h. In another attempt, gemmae were fixed in 3% glutaraldehyde in 1x PBS-T (phosphate buffered saline + 0.1% Tween-20) overnight, subsequently washed in 1x PBS-T, and incubated in aforementioned DAPI solutions in darkness overnight. Furthermore, a modified version of a DAPI staining protocol published for gametophore leaflets and protonemata of *Physcomitrella patens* (Sato et al., 2017) was used. Gemmae were placed in 3.7% formaldehyde in 1x PBS for 30 min. Subsequently gemmae were immersed in 100% MeOH on ice for 10 min. Afterward, gemmae were soaked in 1% Triton X-100 and then stained with the aforementioned DAPI solutions for 30 min. Unfortunately, none of the experimental procedures

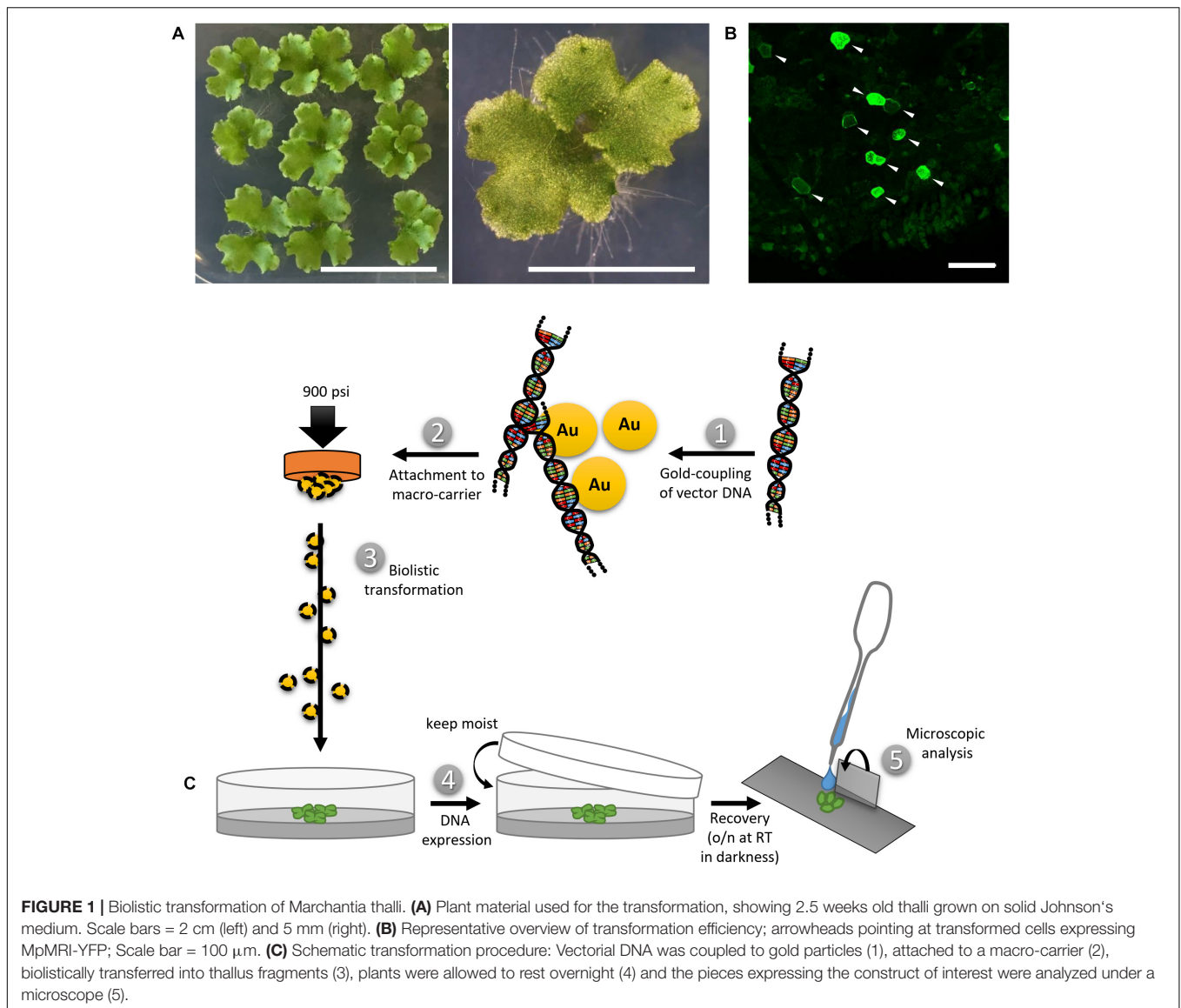
TABLE 2 | Materials, equipment, and chemical solutions needed to perform biolistic transformations and cell stainings on *M. polymorpha*.

Item	Specifications
Plant cultivation	
Johnson's growth medium	According to Ishizaki et al. (2008)
Micropore tape	3M surgical tape (12,5 mm × 9,14 m)
Petri dishes	E.g., round, 9 cm in diameter
Plant growth cabinet	Sanyo MLR-350
Biolistic transformation	
Expression vectors	See Supplementary Table S1
Ethanol, non-denatured	70% and 100% solutions in ddH_2O
Gold microcarriers	1 μm diameter, recommended for PDS-1000-/He systems
Spermidine	0.1 M in ddH_2O
Particle delivery system/gene gun	PDS-1000/He Biolistic® Particle Delivery System (Bio-Rad), including macro-carriers
Cell stainings	
4',6-Diamidino-2-phenylindole (DAPI)	Available from Thermo Fisher Sci. (Cat.# 62248), diluted in 1xPBS-T (for description of alternative solvents see "Methods" section)
Fluorescein diacetate (FDA)	E.g., available from Thermo Fisher Sci. (Cat.# F1303), diluted in acetone
FM4-64 [<i>N</i> -(3-triethylammoniumpropyl)-4-(6-(4-(diethylamino) phenyl) hexatrienyl) pyridinium dibromide]	E.g., available from Thermo Fisher Sci. (Cat.# T3166), diluted in liquid Johnson's growth medium (water-based)
Propidium iodide	E.g., available from Thermo Fisher Sci. (Cat.# P3566), diluted in ddH_2O
Hoechst33342 (bisBenzimide H 33342 trihydrochloride)	E.g., available from Sigma-Aldrich (Cat.# B2261), diluted in ddH_2O
Microscopy and image analysis	
Image analysis software	ImageJ/FIJI V.1.51n
Imaging system	SP8 CLSM (Leica)

described here led to a reliable staining of nuclei by DAPI in viable or fixed epidermal cells of *M. polymorpha* gemmae.

Confocal Laser Scanning Microscopy

The transformed or stained plant material was transferred onto a depression slide supplemented with 300 μL ddH_2O and covered with a 18 × 18 mm cover slip. Rhizoid growth experiments were performed using young gemmae mounted with Johnson's growth medium instead of ddH_2O . Microscopic analysis was performed using a Leica SP8 CLSM with an argon gas laser intensity set at 20%. Fluorophore excitation and fluorescence capture were performed at the wavelength spectra shown in **Supplementary Table S2**. Images were taken using a digital gain of 100% at a resolution of 1024 × 1024 pixels, a pinhole size of 1 AU, and a scan speed of 400–700 Hz using bidirectional confocal scanning and hybrid detectors (HyD). For the capture of multiple fluorophore types sequential or, if suitable, simultaneous scanning was performed. Usage of a laser scanning confocal system is strongly recommended for image capture, as it allows for scanning on multiple focal planes to perform maximum projection, while reducing unspecific background noises (as compared to epifluorescence microscopy).



Data Processing and Analysis

Analysis of all microscopic captions was performed using ImageJ/FIJI (Schindelin et al., 2012), software version 1.51n. Data manipulation included maximum projections from Z-stacks (≤ 20 frames, 1 μ m slice intervals) for some of the markers (as individually mentioned in the figure captions), as well as generation of composite images from separate individual channels.

RESULTS

(A) Fluorescent Protein Markers to Illuminate Cellular Compartments in *Marchantia*

To assess the potential capability of transiently transforming single *Marchantia* thallus epidermal cells, we first chose a

set of proteins whose subcellular localization has been well studied in established model systems such as *Arabidopsis* or tobacco and thus could qualify as reliable subcellular markers in *Marchantia* as well.

Nucleus

We first picked the *Arabidopsis thaliana* INHIBITOR OF CYCLIN-DEPENDENT KINASE 1 (AtICK1)/KIP-RELATED PROTEIN 1 (AtKRP1), which localizes to the nucleus and functions in cell growth, differentiation, and cell cycle progression (Wang et al., 1998; De Veylder et al., 2001; Schnittger et al., 2003; Weinl et al., 2005; Jakoby et al., 2006). Upon biolistic transformation of *Marchantia* thalli, we observed AtKRP1-eCFP protein localization to the nucleus of epidermal cells (Figure 2A). We therefore co-transformed AtKRP1 as a nuclear marker and indicator of successful cell transformation in subsequent experiments.

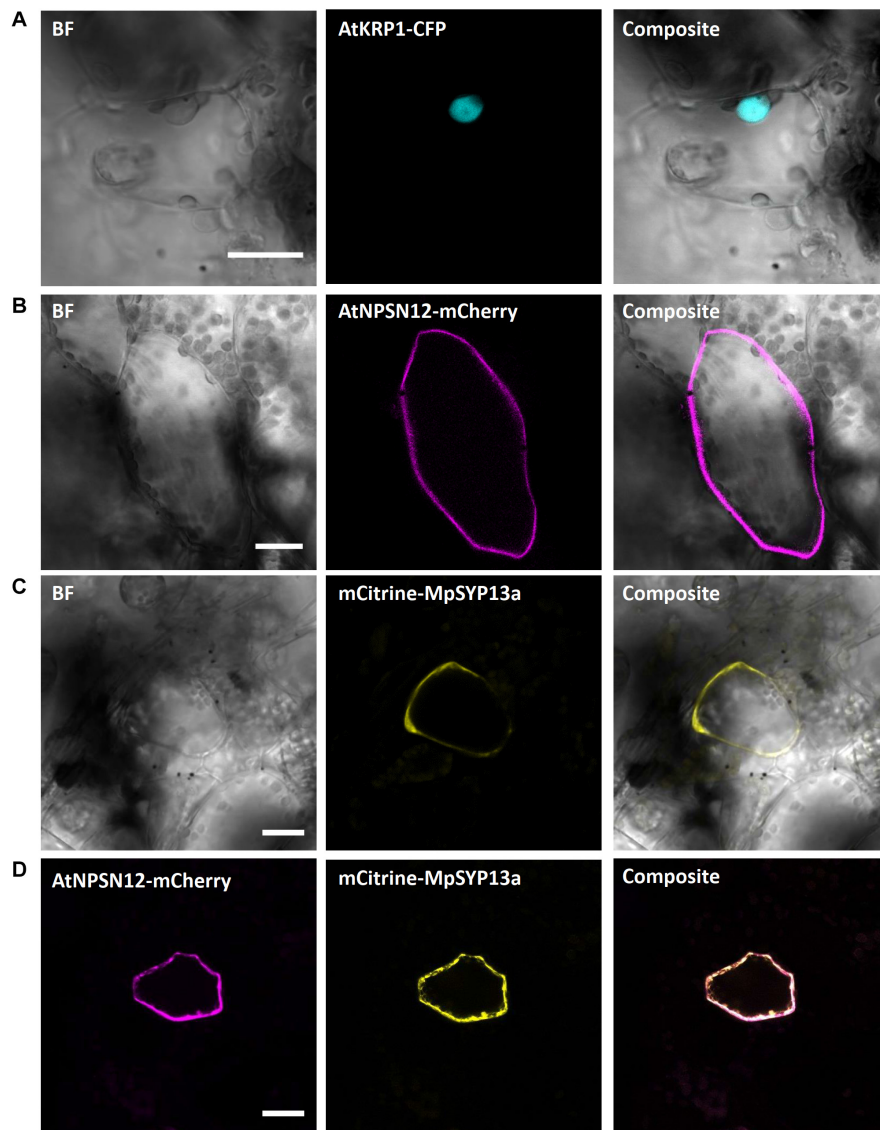


FIGURE 2 | Confirmation of known nuclear and plasma membrane markers. **(A)** The *Arabidopsis* nuclear marker AtKRP1 localizes to the nucleus of *M. polymorpha* epidermal cells. **(B)** The *Arabidopsis* plasma membrane marker AtNPSN12 localizes to the plasma membrane in *Marchantia* epidermal cells. **(C,D)** The *Marchantia* plasma membrane marker MpSYP13a co-localizes with AtNPSN12. All scale bars = 20 μ m. BF, bright field.

Plasma Membrane

As a second potential marker, we chose the *Arabidopsis thaliana* NOVEL PLANT SNARE 12 (AtNPSN12), which represents a non-polar plasma membrane-localized protein commonly used as plasma membrane marker (Alassimone et al., 2012; Kirchhelle et al., 2016). Biolistically transformed *Marchantia* thallus epidermal cells showed AtNPSN12-mCherry fluorescence at the cell periphery consistent with plasma membrane localization (**Figure 2B**). To confirm this localization, we co-transformed AtNPSN12-mCherry with the known *Marchantia* plasma membrane marker mCitrine-MpSYP13a (Kanazawa et al., 2016) (**Figure 2C**). As single and co-bombardments with AtNPSN12 showed (co)localization to the plasma membrane,

we conclude that AtNPSN12-mCherry and mCitrine-MpSYP13a are both suitable plasma membrane markers for *Marchantia* epidermal cells (**Figure 2D**).

Receptor-like kinases of the Malectin-like receptor (MLR) subfamily have been the subject of intensive research in the past years given their multitude of functions in plant development and immunity signaling (Franck et al., 2018a). The plasma membrane localized MLRs ANXUR1 and 2 (AtANX1/2) control cell wall integrity during pollen tube growth (Boisson-Dernier et al., 2009; Miyazaki et al., 2009) and negatively regulate plant immune responses in *Arabidopsis* (Mang et al., 2017). During pollen tube growth control, AtANX1/2 act genetically upstream of the cytosolic and plasma membrane-attached receptor-like

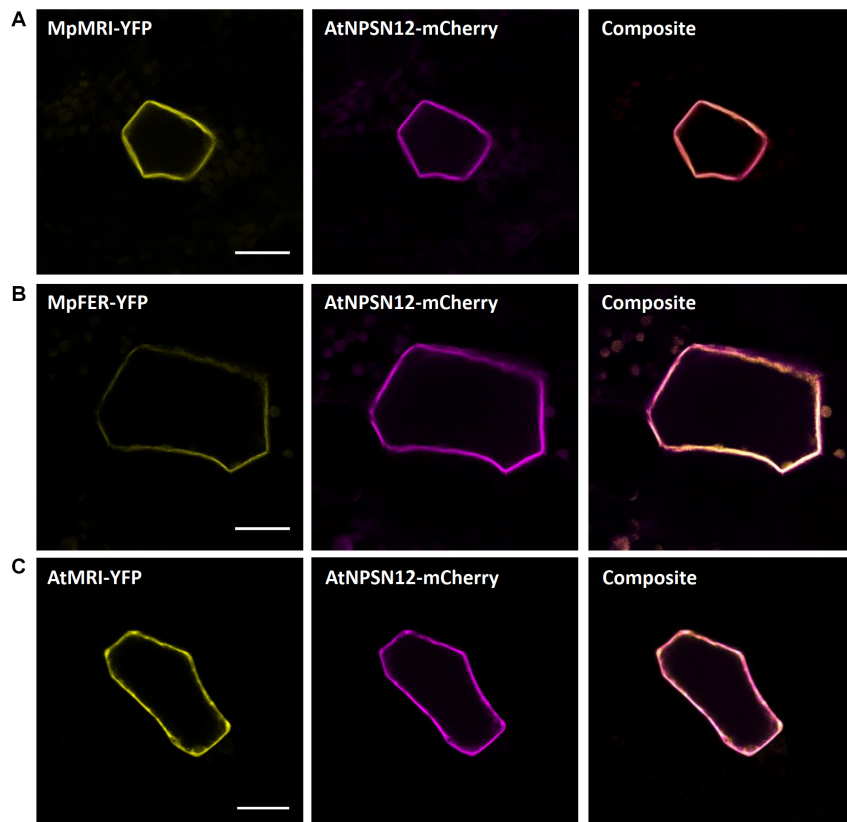


FIGURE 3 | Plasma membrane markers for Marchantia research. MpMRI (**A**), MpFER (**B**) and AtMRI (**C**) all localized to the plasma membrane of *M. polymorpha* thallus epidermal cells. All three constructs co-localized with the plasma membrane marker AtNPSN12. All scale bars = 20 μm .

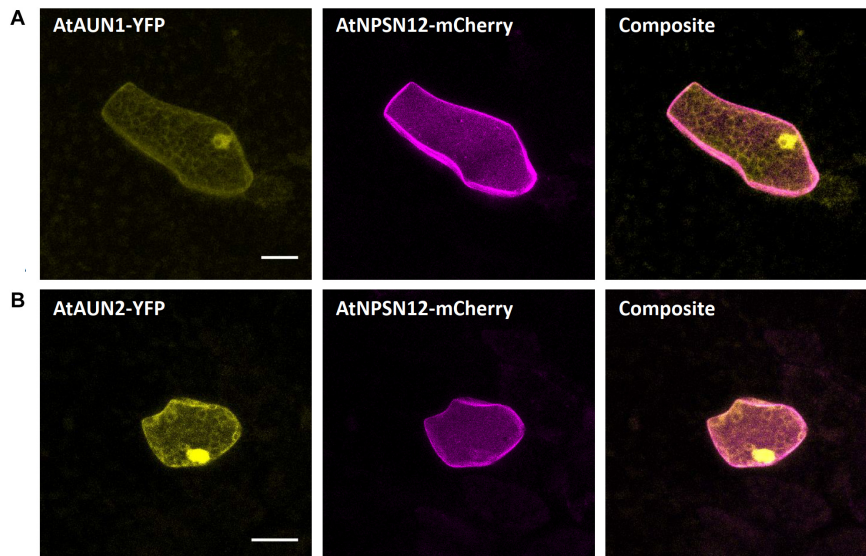


FIGURE 4 | Nucleocytoplasm markers for Marchantia research. Both, AtAUN1 (**A**) and AtAUN2 (**B**) localized to the cytoplasm and nucleus of *M. polymorpha* thallus epidermal cells, consistent with observations in *A. thaliana* (Franck et al., 2018b). The constructs were co-bombarded with plasma membrane marker AtNPSN12. All scale bars = 20 μm . Pictures show maximum projections of z-stack captions, hence the appearance of the 'cytoplasmic noise' signal for AtNPSN12-mCherry (see "Materials and Methods" section for details).

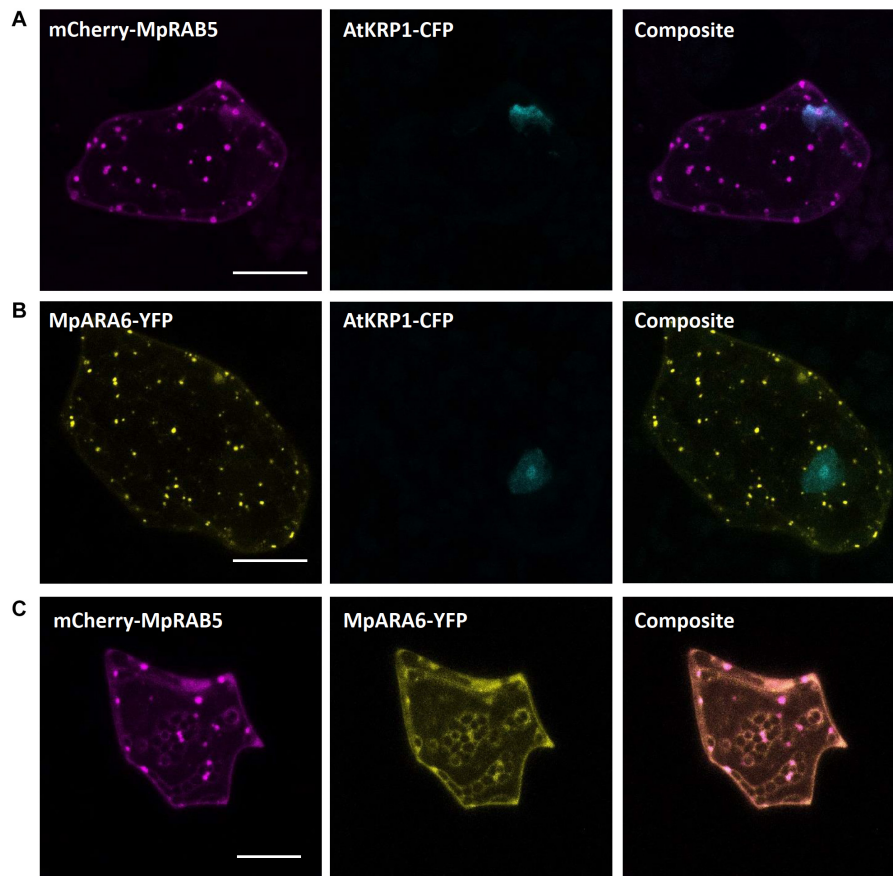


FIGURE 5 | Endosomal markers for Marchantia research. Both, MpRAB5 (**A**) and MpARA6 (**B**) localized to punctuate intracellular structures of *M. polymorpha* thallus epidermal cells, likely representing endosomes. The constructs were co-bombarded with nuclear marker AtKRP1. The endosomal markers MpRAB5 and MpARA6 also show clear co-localization (**C**). All scale bars = 20 μ m. Pictures show maximum projections of z-stack captions (see “Materials and Methods” section for details).

cytoplasmic kinase of the PTI1-like family, AtMRI, while the AtANX1 homolog AtFERONIA (AtFER) acts upstream of AtMRI during root hair growth control (Boisson-Dernier et al., 2015). We showed recently that tip-growth control in Marchantia rhizoids relies on an evolutionarily conserved signaling module comprised of the unique Marchantia MLR MpFER and its downstream component and unique Marchantia PTI1-like MpMRI (Westermann et al., 2019). We transiently co-expressed the fluorescent protein fusions AtMRI-YFP, MpFER-YFP, and MpMRI-YFP with AtNPSN12-mCherry. While MpFER-YFP showed signal exclusive to the plasma membrane, AtMRI and MpMRI displayed plasma membrane localization with traces in the cytoplasm as reported before (Figure 3) (Boisson-Dernier et al., 2015; Westermann et al., 2019).

Noteworthy, we also wanted to test expressing the plasma membrane localized Arabidopsis MLRs in Marchantia and thus co-transformed AtANX1-RFP with mCitrine-MpSYP13a and AtFER-Citrine with AtNPSN12-mCherry. Intriguingly, while many cells expressed the plasma membrane markers mCitrine-MpSYP13a and AtNPSN12-mCherry, a great majority of them did not show expression of either AtANX1 or AtFER

(Supplementary Figures S1A,B). This suggests that, unlike MpFER, the Arabidopsis MLRs fused to single fluorescent tag cannot be expressed in Marchantia epidermal cells. Thus, we next tried to express AtFER with a triple Citrine tag instead of a single one. It resulted in many Citrine-expressing cells but mostly in the cytoplasm, with no hints of plasma membrane localization (Supplementary Figure S1C). These results indicate that fusion of long protein tags may prevent transmembrane receptor kinases such as MLRs to be correctly integrated into cellular membranes. To check if this was specifically due to Arabidopsis proteins or to certain protein families, we co-expressed MpFER-3xCitrine with MpFER-TdTomato and MpMRI-3xCitrine with MpMRI-RFP (Supplementary Figures S1D, E). Interestingly, the 3xCitrine tag did not perturbate the cytosolic and plasma membrane localization of MpMRI, as MpMRI-3xCitrine co-localized with MpMRI-RFP at the cell periphery. However, while MpFER-TdTomato exhibited PM localization, MpFER-3xCitrine-derived signal was clearly present in the cytoplasm. Therefore, for some plasma membrane-localized protein families, fusion with a triple tag can lead to localization artifacts, and the use of single tag is thus recommended by default. Why MpFER but neither AtFER

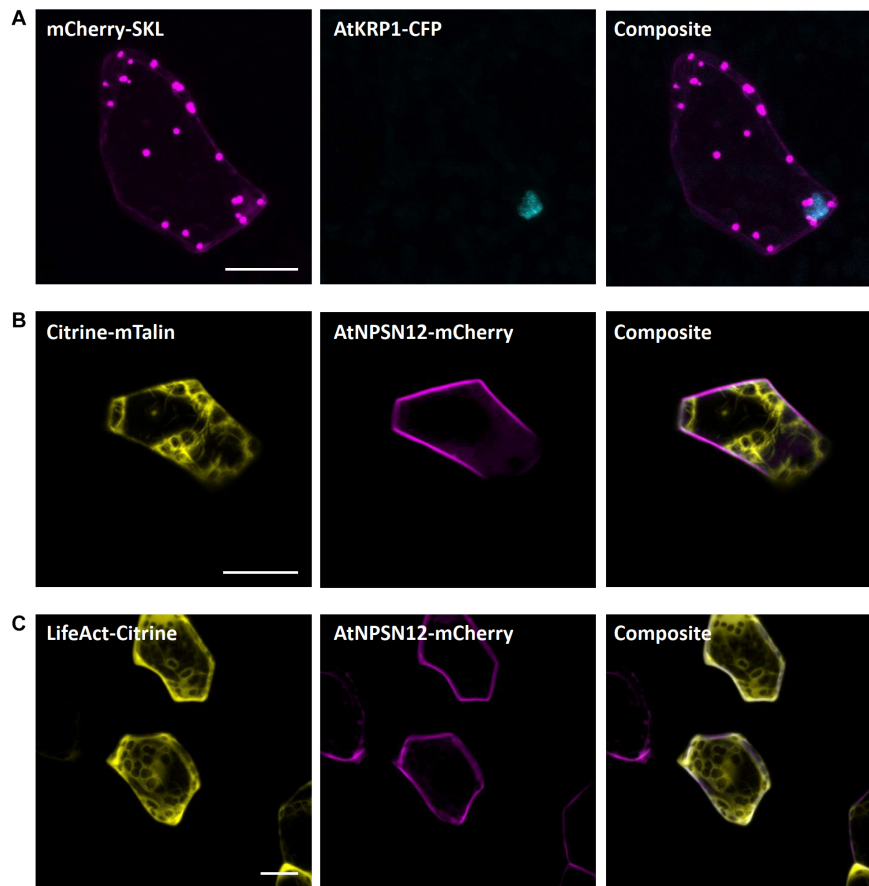


FIGURE 6 | Peroxisomal and actin filaments markers for Marchantia research. **(A)** The SKL-target sequence tagged to mCherry localized to single intracellular foci of *M. polymorpha* thallus epidermal cells, likely representing peroxisomes. mCherry-SKL was co-bombarded with nuclear marker AtKRP1. The actin filament markers **(B)** Citrine-mTalin and **(C)** LifeAct-Citrine were co-bombarded with plasma membrane marker AtNPSN12-Mcherry. All scale bars = 20 μm . Pictures show maximum projections of z-stack captions (see “Materials and Methods” section for details).

nor AtANX1 can be expressed in Marchantia thallus epidermis remains puzzling.

Cytoplasm

The *A. thaliana* type-one protein phosphatases (TOPP) AtATUNIS1/2 (AtAUN1/2) have recently been reported as negative regulators of cell wall integrity maintenance during Arabidopsis tip-growth (Franck et al., 2018b). The nucleocytoplasmic localization of AtAUN1-YFP and AtAUN2-YFP was demonstrated in Arabidopsis pollen tubes and leaf epidermal cells (Franck et al., 2018b). In Marchantia epidermal cells, expression of AtAUN1/2-YFP led to a comparable nucleocytoplasmic localization, as opposed to the co-expressed plasma membrane localized AtNPSN12-mCherry fusion (Figure 4), therefore qualifying these phosphatases as reliable Marchantia nucleocytoplasmic markers.

Endosomes

As for endosomal compartments, we chose two Ras-related in brain (RAB) GTPases, the canonical MpRAB5 and the plant-unique MpARA6, that were recently described in *M. polymorpha*.

Both proteins were successfully expressed in stably transformed lines and co-localized to endosomal punctate structures stained by FM1-43 (Minamino et al., 2018). Upon biolistic co-transformation of the protein fusions mCherry-MpRAB5 and MpARA6-eYFP with the nuclear marker AtKRP1-eCFP (Figures 5A,B), we found a comparable localization in punctate structures for both markers. Moreover, both GTPases strongly co-localized with each other (Figure 5C) showing that MpRAB5 and MpARA6 are suitable endosomal markers also for transient transformation studies.

Peroxisomes

The carboxyl-terminal amino acid sequence serine–lysine–leucine (SKL) is well known as the consensus peroxisomal targeting sequence 1 (PTS1) and is sufficient to induce protein targeting and import to peroxisomes. SKL was first shown to be able to signal protein import into peroxisomes of mammalian cells (Gould et al., 1989) but later was also found to be functional in yeast and plants (Keller et al., 1991). In Arabidopsis, SKL motif fused to fluorescent tags is frequently used as a peroxisomal marker (Mathur et al., 2002; Kim et al., 2013; Rodríguez-Serrano

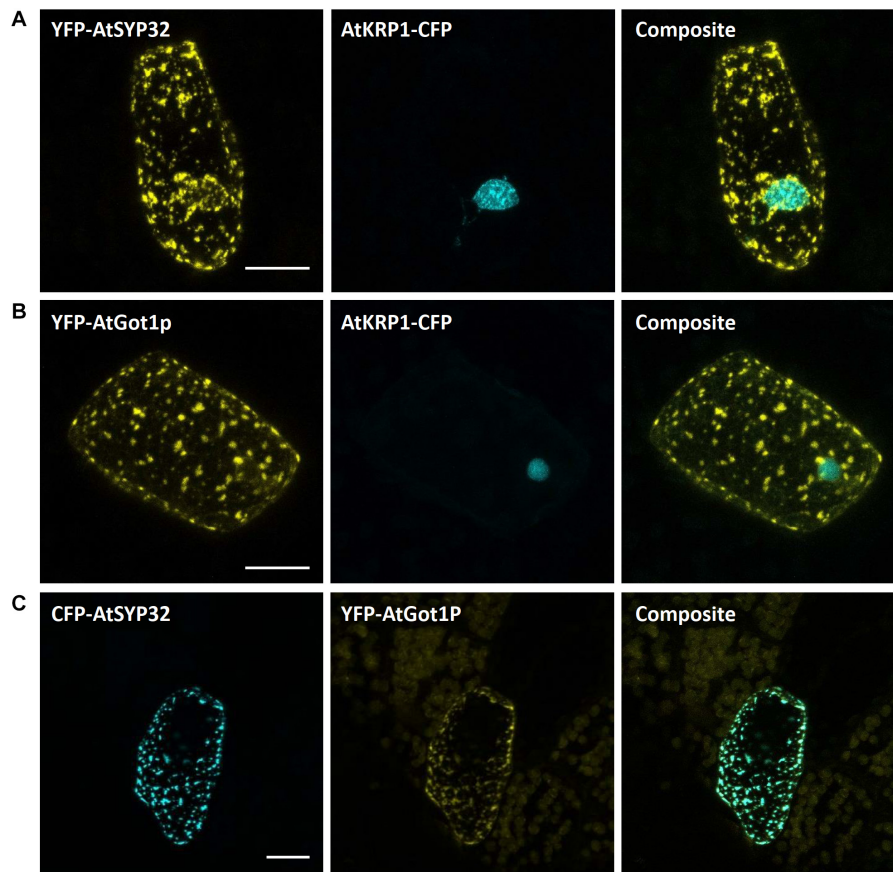


FIGURE 7 | Golgi markers for Marchantia research. The Arabidopsis Golgi markers AtGot1p (**A**) and AtSYP32 (**B**) localize to the Golgi apparatus of *M. polymorpha* epidermal cells. The constructs were co-bombarded with nuclear marker AtKRP1. (**C**) The Golgi markers AtGot1p and AtSYP32 show clear co-localization. All scale bars = 20 μ m. BF, bright field.

et al., 2016). In *M. polymorpha*, SKL targeting was utilized for evaluation of CRISPR-Cas9 modules (Konno et al., 2018). In transiently transformed *M. polymorpha* cells, we also found a clear and distinct localization of mCherry-SKL in punctate structures, likely representing peroxisomes (**Figure 6A**).

Actin Filaments

Both the LifeAct peptide - a short peptide of 17 amino acids - and the C-terminal 197 amino acids of mouse talin are known to bind to filamentous actin (Kost et al., 1998; Riedl et al., 2008). Therefore, to visualize the actin filaments in Marchantia epidermal cells, we used the Citrine-mTalin and LifeAct-Citrine reporters described previously (Kimura and Kodama, 2016). As in stably transformed Marchantia lines (Kimura and Kodama, 2016), both markers successfully revealed the actin filament networks around chloroplasts in epidermal cells (**Figures 6B,C**).

Golgi Apparatus

As potential markers for the Golgi apparatus, we selected the Arabidopsis proteins SYNTAXIN OF PLANTS 3 (AtSYP3) and the GOLGI TRANSPORT 1 p homolog (AtGot1p). Both proteins have been shown to localize to the Golgi apparatus

(Conchon et al., 1999; Uemura et al., 2004) and are reliable Golgi markers for Arabidopsis, as being part of the Wave line multicolor marker set for membrane compartments (WAVE22 and WAVE18, respectively; Geldner et al., 2009). Upon transient biolistic expression of eYFP-AtSYP3 and eYFP-AtGot1p in *M. polymorpha*, a distinct and comparable localization pattern of both proteins, likely representing the Golgi apparatus, was visible (**Figures 7A,B**). Furthermore, upon co-expression of eCFP-AtSYP3 and eYFP-AtGOT1p, we also found perfect co-localization (**Figure 7C**) confirming that both markers are reliable to illuminate the Golgi in Marchantia.

mRNA Processing Bodies

mRNA processing bodies (p-bodies), have been found to play a crucial role in mRNA processing comprising deadenylation, decapping, degradation, mRNA storage and mRNA quality control (thoroughly reviewed for *A. thaliana* in Maldonado-Bonilla, 2014). As p-bodies markers, we chose the *Arabidopsis thaliana* DECAPPING PROTEIN 1 (AtDCP1) and AtDCP2, whose function has been well studied in the past years (Xu et al., 2006; Xu and Chua, 2009; Steffens et al., 2015; Bhasin and Hülskamp, 2017). Upon transformation of the protein

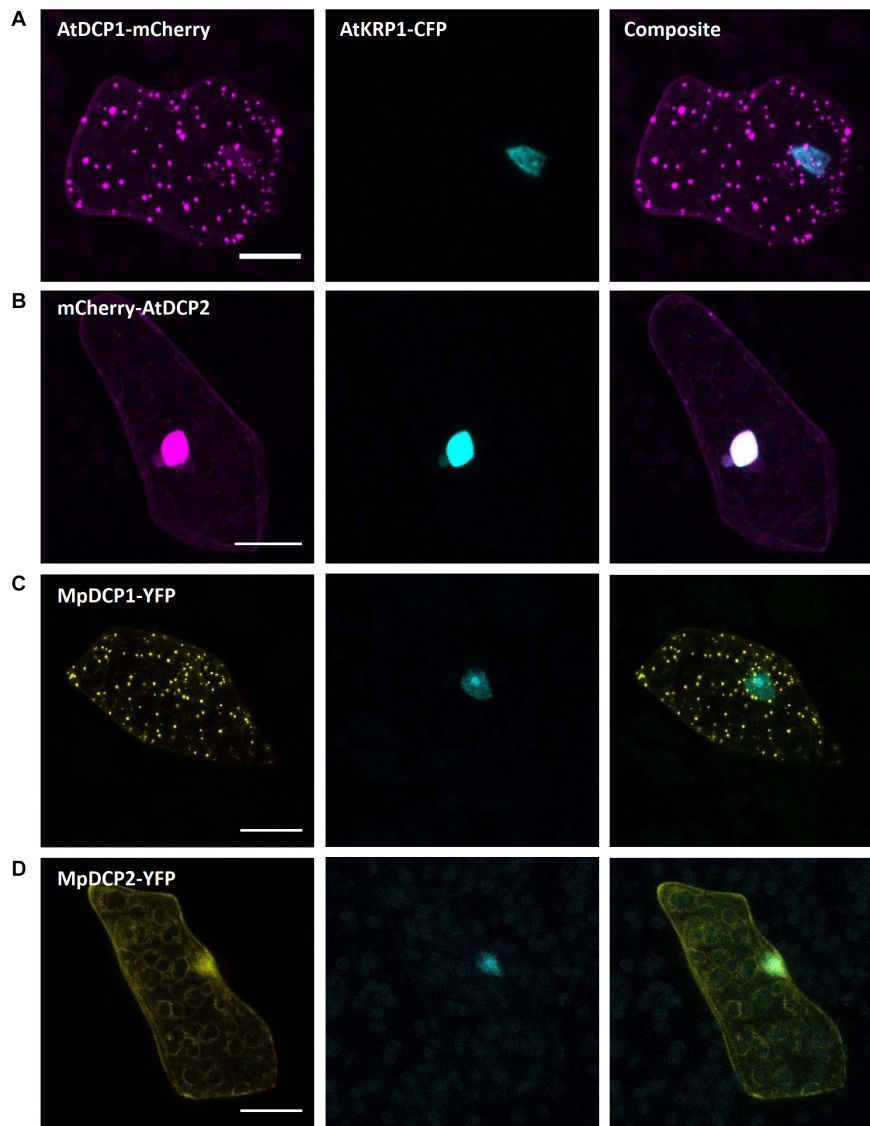


FIGURE 8 | Marchantia p-body markers. Both, AtDCP1 (**A**) and MpDCP1 (**C**) localized to intracellular dot-like structures, that likely represent p-bodies. In contrast, AtDCP2 (**B**) and MpDCP2 (**D**) localized to the cytoplasm, consistent with former observations (Motomura et al., 2015). Additionally, both, AtDCP2 and MpDCP2 showed a nuclear localization, co-localizing with the nuclear signal of AtKRP1. The constructs were co-bombarded with nuclear marker AtKRP1. Scale bar = 20 μ m. Pictures show maximum projections of z-stack captions (see “Materials and Methods” section for details).

fusion AtDCP1-mCherry we found a comparable expression in dot-like structures, likely representing p-bodies (**Figure 8A**). In contrast, transformation of mCherry-AtDCP2 revealed a diffused expression throughout the cytoplasm and in the nucleus (**Figure 8B**), as reported in Arabidopsis in the absence of stress (Motomura et al., 2015). Therefore, we assume that AtDCP2 is also generally localized in the cytoplasm and nucleus in *M. polymorpha* and is only recruited to p-bodies upon stress conditions (Motomura et al., 2015).

The similar localization of AtDCP1/2 in Arabidopsis (Iwasaki et al., 2007; Motomura et al., 2015) and Marchantia suggests that the function of DCPs in mRNA processing has been evolutionarily conserved. To assess whether the two

Marchantia DCP-homologs MpDCP1/2 localize similarly as their Arabidopsis counterparts, we transformed different combinations of fluorescent fusions (MpDCP1-mCherry, MpDCP1-eYFP, MpDCP2-mCherry, MpDCP2-eYFP). As anticipated, MpDCP1 displayed a dot-like localization pattern similar to AtDCP1, while MpDCP2 exhibited an AtDCP2-like nucleocytoplasmic localization (**Figures 8C,D**).

(B) Bimolecular Fluorescence Complementation

Based on former reports of AtDCP1 to regulate mRNA decay and to recruit further functionally relevant proteins, such as

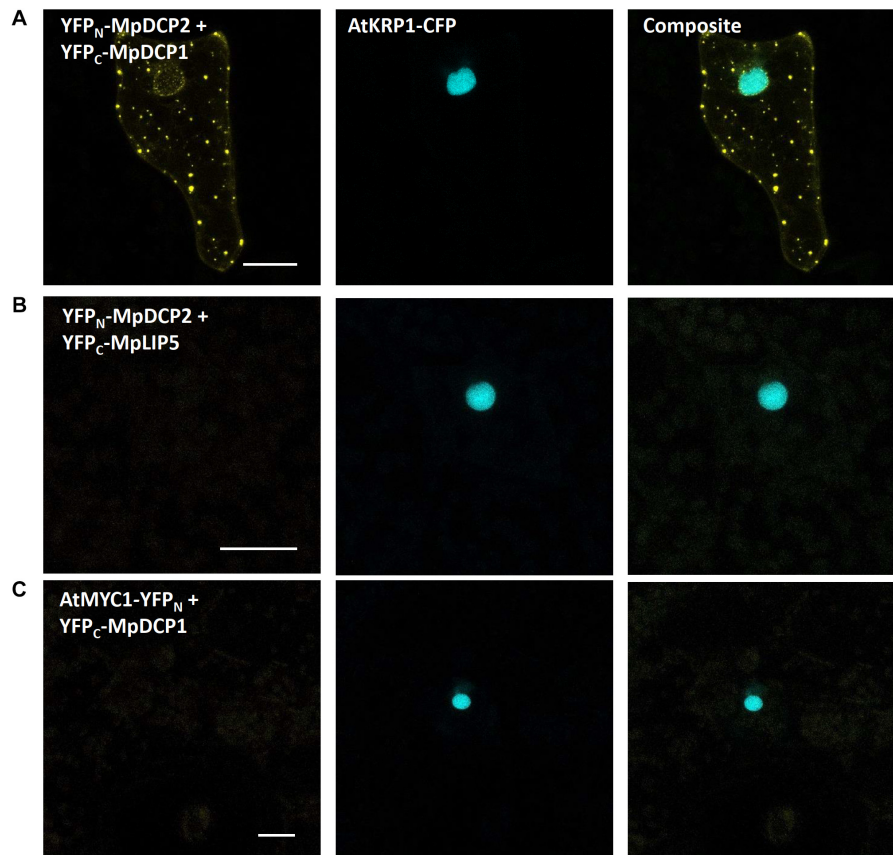


FIGURE 9 | Bimolecular fluorescent complementation assays showing interaction between MpDCP1 and MpDCP2. **(A)** Co-transformation of split-YFP fusion constructs of MpDCP1 and MpDCP2 result in a fluorescence signal in dot-like foci, indicating protein–protein interaction in p-bodies. **(B)** Co-bombardment of split-fusions with MpDCP2 and the unrelated MpLIP5 protein were used as a negative control. **(C)** We also co-bombarded split-versions of MpDCP1 and unrelated AtMYC1, which also led to the absence of any fluorescence signal. The constructs were co-bombarded with nuclear marker AtKRP1. Scale bar = 20 μm . Pictures show maximum projections of z-stack captions (see “Materials and Methods” section for details). See also **Supplementary Figure S2** for other controls.

AtDCP2, to p-bodies (Iwasaki et al., 2007; Motomura et al., 2015), as well as our own observations (see above), we selected MpDCP1/2 as promising candidates to assess the feasibility of studying protein–protein interactions in *M. polymorpha* via bimolecular fluorescence complementation (BiFC). The BiFC technique relies on the co-expression of two proteins fused to the N- or C-terminal part of a fluorescent reporter (e.g., -YFP_N and -YFP_C, respectively). Upon physical interaction of the two tagged proteins of interest, the N- and C-terminal parts of the reporter can reconstitute a functional fluorescent protein. Capture of the respective fluorescent signal thus is used as an indicator for protein–protein interaction. For BiFC to be meaningful, the co-transformation of both reporter halves must lead to regular and frequent co-expression, which is the case for Marchantia thallus transient biolistic transformation as it reaches, in our hands, 74% on average (see “Materials and Methods” section and **Supplementary Table S3**). The physical interaction of AtDCP1/2 was foremost reported in *in vitro* pull-down assays (Xu et al., 2006) and later independently confirmed by BiFC in tobacco mesophyll protoplasts (Weber et al., 2008).

Interestingly, upon co-expression of YFP_N-MpDCP2 and YFP_C-MpDCP1, together with the nuclear marker AtKRP1-eCFP, we could observe a clear and specific YFP signal in dot-like structures, suggesting that MpDCP1/2 are capable of interacting physically in p-bodies of Marchantia epidermal cells (**Figure 9A**). To exclude the possibility of false positive signals (Kodama and Hu, 2012) in our experimental setup we also transformed YFP_N-MpDCP2 and YFP_C-MpDCP1 with YFP_C-MpLYST interacting protein 5 (MpLIP5) and AtMYC related protein 1 (AtMYC1)-YFP_N tags, respectively. Expression of both vector combinations led to the absence of a YFP signal in cells expressing AtKRP1-eCFP (**Figures 9B,C**), indicating that the observed interaction between MpDCP1 and MpDCP2 is specific. The integrity of YFP_C-MpLIP5 was confirmed by co-expression with the Marchantia homolog of a known interactor of LIP5 in Arabidopsis - MpSuppressor of K⁺ Transport Growth Defect1 (MpSKD1) (Haas et al., 2007), N-terminally fused to YFP_N, showing a clear YFP signal in punctate structures consistent with localization to p-bodies (**Supplementary Figure S2A**). The integrity of AtMYC1-YFP_N was shown by a BiFC interaction in the nucleus with its known interaction partner

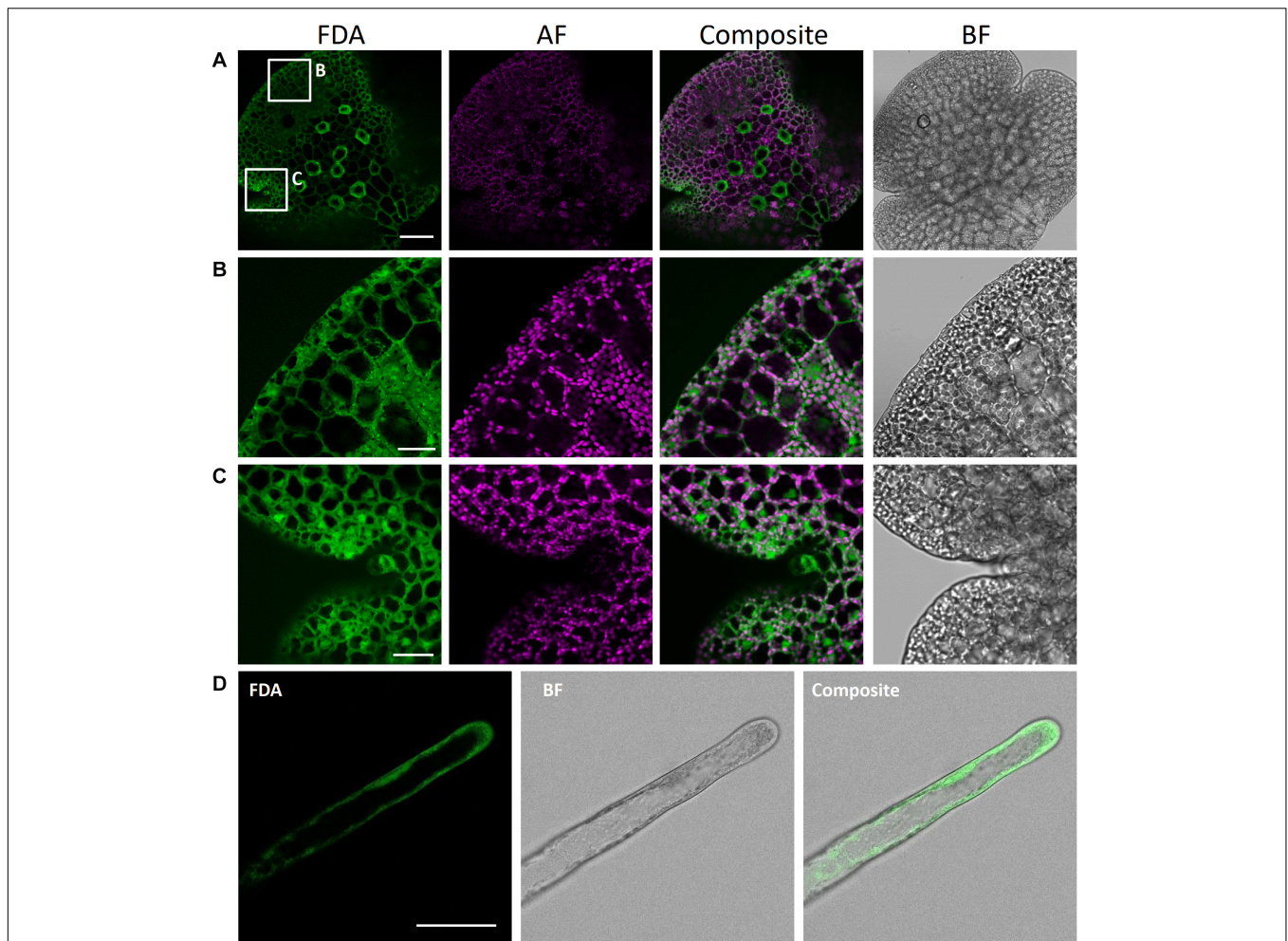


FIGURE 10 | Fluorescein diacetate staining of different *M. polymorpha* cell types. **(A)** Whole-thallus staining, scale bar = 100 μm , with close-up captures of **(B)** a distal thallus fragment, scale bar = 30 μm , and **(C)** a meristematically active apical notch, scale bar = 30 μm . All three images show localization of FDA to the cytoplasm, as contrasted by absence of FDA-specific fluorescence in the vacuole and autofluorescent (AF) chloroplasts. Pictures show maximum projections of z-stack captures (see “Materials and Methods” section for details). **(D)** FDA staining of a Tak-1 rhizoid of a 5-day-old gemmaling. BF, bright field. Scale bar = 50 μm .

AtTRANSPARENT TESTA GLABRA1 (TTG1) (Zimmermann et al., 2004; Zhao et al., 2012; control used in Steffens et al., 2017), C-terminally fused to YFP_C (**Supplementary Figure S2B**). In conclusion, our results show that BiFC is functional in *Marchantia* and can be used to quickly assess protein–protein interactions *in vivo*.

(C) Staining Intracellular Structures in *M. polymorpha*

For the visualization of a cell and the investigation of cellular architecture and dynamics, it is crucial to have several quick and reliable staining methods for live cell imaging at hand. Therefore, we tested some standard staining procedures to label intracellular compartments and cellular structures (including the plasma membrane, cytoplasm, cell wall, and nucleus) in *M. polymorpha* gemmae that have been established for other plants but lacking ready-to-use protocols for *Marchantia*.

Fluorescein Diacetate (FDA) for Cytoplasm Staining of Living Cells

Fluorescein diacetate is a cell-permeable, *per se* non-fluorescent esterase substrate. As soon as it passes the plasma membrane, it is hydrolyzed by esterases in the cytoplasm of viable cells (Rotman and Papermaster, 1966). Thereby, FDA is converted to a negatively charged, green-fluorescent fluorescein unable to either cross back the plasma membrane or pass the tonoplast and thus it accumulates in the cytoplasm. Owing to these properties, FDA is suitable for cell viability assays and can be used as a negative stain for vacuoles. FDA staining has been reliably used for testing *Arabidopsis* root hair and guard cell viability (Schapire et al., 2008; Hao et al., 2012), to visualize vacuoles in root hairs (Saedler et al., 2009) and trichomes (Mathur et al., 2003), and to study pathogen response (Jones et al., 2016), as well as to assess *Marchantia* protoplast viability (Sugawara and Fukukawa, 1995).

Here, we successfully utilized FDA to stain the cytoplasm of rhizoids and epidermal cells in young gemmae (**Figure 10**).

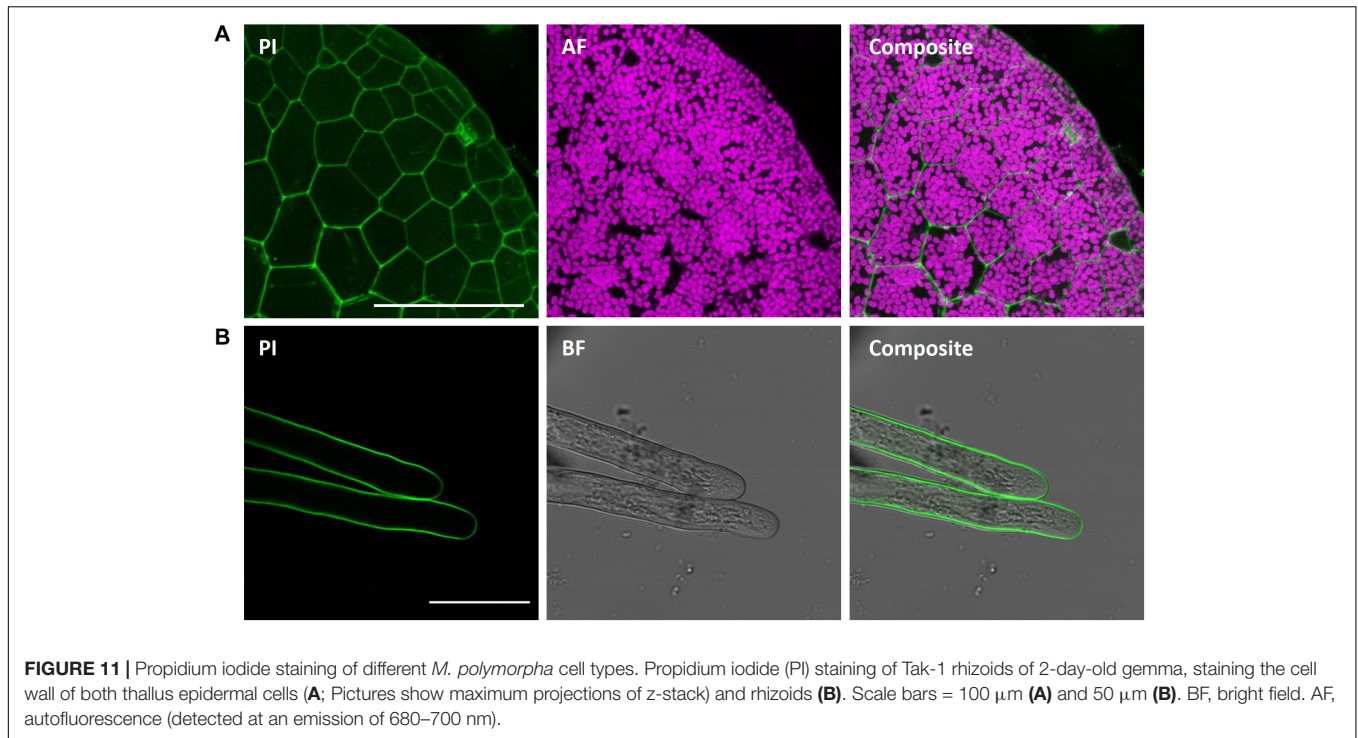


FIGURE 11 | Propidium iodide staining of different *M. polymorpha* cell types. Propidium iodide (PI) staining of Tak-1 rhizoids of 2-day-old gemma, staining the cell wall of both thallus epidermal cells (**A**; Pictures show maximum projections of z-stack) and rhizoids (**B**). Scale bars = 100 μm (**A**) and 50 μm (**B**). BF, bright field. AF, autofluorescence (detected at an emission of 680–700 nm).

FDA showed a strong, green fluorescence already after a short incubation time of 10 min, demonstrating the viability of rhizoids and epidermal cells. We here present FDA as a tool to be readily used for visualization of the cytoplasm in *M. polymorpha*. As it is not able to pass the tonoplast, it can also be used to detect vacuolar architecture, especially in rhizoids, where vacuolar volume was clearly visible after staining with FDA (**Figure 10D**).

Propidium Iodide for Cell Wall Staining

Propidium iodide (PI) is an intercalating, red-fluorescent cell dye. It penetrates damaged cell membranes and visualizes nuclei of dead cells by intercalating DNA with low base preference. However, PI cannot pass intact cell membranes and thus is excluded from viable cells, while remaining fluorescent. Therefore, PI can also readily be used to visualize cell wall of living cells. In Arabidopsis, PI is regularly utilized for counterstaining of cell walls (Takano et al., 2002; Ubeda-Tomás et al., 2009), such as for viability assays, frequently combined with FDA (Shahriari et al., 2010; Kong et al., 2018).

We here show successful PI staining of cell walls of *M. polymorpha* (**Figure 11**), in agreement with former reports (Delmans et al., 2017; Jones and Dolan, 2017; Thamm et al., 2020). Strong fluorescence was observed already after short incubation times of 10 min. PI reliably stained the cell walls of living epidermal cells (**Figure 11A**) and rhizoids (**Figure 11B**) and thus can reveal cell shape and size. This staining was non-toxic as stained rhizoids kept elongating, thereby revealing the usefulness of PI staining for studying rhizoid tip-growth (**Supplementary Video S1**).

Nuclei of *M. polymorpha* Cannot Be Reliably Stained With 4',6-Diamidino-2-Phenylindole (DAPI)

DAPI is one of the most common DNA fluorochromes enabling staining and visualization of nuclei of dead but also viable cells, as it is able to pass cell membranes – however, often with weak effectiveness. Upon excitation with ultraviolet light, DAPI emits blue fluorescence at a maximum of 461 nm. DAPI binds stoichiometrically to adenine-thymine rich regions of DNA. DAPI also has a weak binding capacity to RNA, however emission is then shifted to 500 nm. Thus, DAPI is frequently utilized not only to visualize nuclei in trichomes, epidermal pavement cells or root cells (Kirik et al., 2001; Lee et al., 2006; Spitzer et al., 2006), but also to quantify DNA content in Arabidopsis, being a reliable tool to discover endoreduplication (Schnittger and Hülskamp, 2007; Bramsiepe et al., 2010; Bhosale et al., 2018). Kondou et al. (2019) report a functional DAPI staining of nuclei in wholemount samples of fixed epidermal cells of *M. polymorpha*. In this study, we tested staining of fixed (i.e. after a modified version of the protocol by Kondou et al., 2019) but also of viable thallus epidermal cells of Marchantia. Surprisingly, despite usage of gemmae at different developmental stages, short to long DAPI incubation periods, preceding and subsequent de-staining steps using EtOH, different methods of fixation (for more details see “Materials and Methods” section), we were unable to stain and visualize nuclei of Marchantia with DAPI (**Supplementary Figure S3**). In our hands, DAPI accumulated on cell walls and to a weaker extent in the cytoplasm but did not enter the nucleus. To demonstrate functionality of the used DAPI solution, we stained Arabidopsis leaves in parallel (**Supplementary Figure S3**), showing strong and distinctive visualization of nuclei. Staining of DNA by PI after fixation

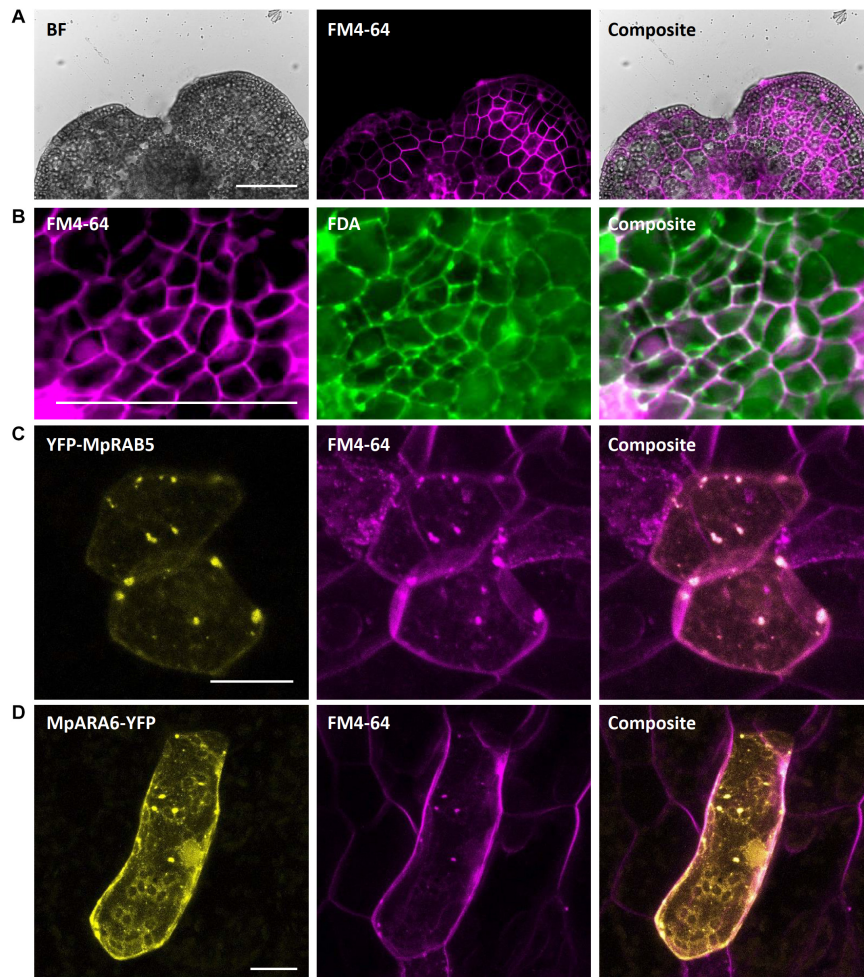


FIGURE 12 | FM4-64 staining of *M. polymorpha* thallus epidermal cells. **(A)** FM4-64 staining of a 2-day-old Tak-1 gemmaling, staining the plasma membrane of thallus epidermal cells. **(B)** Co-staining of FM4-64 and FDA showing opposing plasma membrane- and cytoplasm-localized fluorescence signal. **(C)** Transient expression of eYFP-MpRAB5 and MpARA6-eYFP **(D)**, co-stained with FM4-64. Co-localizing signals represent endosomal structures. BF, bright field. FDA, fluorescein-diacetate. Scale bars: 100 μm **(A,B)** and 20 μm **(C,D)**.

also failed in our hands (data not shown). Additionally, we stained young gemmae with Hoechst33342 for 10 min at 10 mg/L concentration, but it also failed in our hands to consistently stain nuclei. It remains to be elucidated, why nuclei of *M. polymorpha* seem to be hardly accessible to DNA fluorochromes. Until then, we either suggest to use a protein marker localizing in nuclei (e.g., AtKRP1) and to generate stably expressing Marchantia lines if needed; or to visualize S-phase nuclei with 5-ethynyl-2'-deoxyuridine (EdU) staining, as reports show its functionality in *M. polymorpha* (Furuya et al., 2018; Busch et al., 2019).

FM4-64 Staining for Visualization of Plasma Membrane and Endocytic Vesicles

The lipophilic steryl dye FM4-64 ((3-triethylammoniumpropyl)-4-(6-(4-(diethylamino)-phenyl)-hexatrienyl) pyridinium-dibromide) is commonly used as marker for the outer leaf of the cellular plasma membrane. Staining of young gemmae with FM4-64 resulted in a clear fluorescence signal at the

cellular boundaries, likely representing the plasma membrane (**Figure 12A**). Upon co-staining with FDA, the FM4-64-specific plasma membrane signal at the cell periphery was clearly distinct from the cytoplasmic FDA signal (**Figure 12B**). Additionally, we stained Marchantia thallus fragments, transiently transformed with eYFP-MpRAB5 or MpARA6-eYFP, with the FM4-64 dye. The eYFP- and FM4-64-derived fluorescent signals co-localized at the punctuate endosomal structures (**Figures 12C,D**). Altogether, these findings support FM4-64 as a reliable marker dye to label the outer cellular membrane and endosomes via single or co-staining in Marchantia.

CONCLUDING REMARKS

We here present a comprehensive and reliable toolkit for visualization of intracellular architecture and dynamics in *M. polymorpha*, an emerging model system used to study

land plant evolution. All methods described are based on standard techniques used in other systems and can be executed and analyzed within 1–2 working days, therefore allowing time-efficient analysis of basic intracellular traits, such as organelle organization and cell architecture, both in fixed and viable cells. The possibility to mark viable cells additionally allows their analysis in live-imaging setups, as we demonstrate with growing rhizoids stained with PI. A comprehensive list of transiently expressed markers covering the majority of intracellular organelles and structures, allows fast assessment of aforementioned intracellular dynamics in viable cells, but also provides a quick possibility for initial tests of functionality and correct localization of cloned fluorescent constructs before committing to comparatively time-costly stable plant transformation. Finally, we demonstrate the BiFC system to be functional in *Marchantia* epidermal cells, thus representing a quick and straightforward technique to test for protein–protein interactions *in vivo*, which should be confirmed with other protein–protein interaction assays such as Yeast-2-Hybrid-like, FRET-FLIM and protein pulldown approaches. Altogether, we provide a series of quick and useful techniques to exploit the potential of an emerging model system to the maximum extent possible.

DATA AVAILABILITY STATEMENT

The raw data supporting the conclusions of this article will be made available by the authors, without undue reservation.

AUTHOR CONTRIBUTIONS

JW, EK, MH, and AB-D conceived the experiments. JW, EK, RL, and AB-D performed the experiments. JW, EK, and AB-D analyzed the data. JW and EK wrote the manuscript with contributions of MH and AB-D. All authors contributed to the article and approved the submitted version.

FUNDING

This research was partly funded by a short-term stipend of the Deutscher Akademischer Austauschdienst (DAAD) to JW; the

REFERENCES

- Alassimone, J., Roppolo, D., Geldner, N., and Vermeer, J. E. M. (2012). The endodermis-development and differentiation of the plant's inner skin. *Protoplasma* 249, 433–443. doi: 10.1007/s00709-011-0302-5
- Bhasin, H., and Hülskamp, M. (2017). ANGUSTIFOLIA, a Plant Homolog of CtBP/BARS localizes to stress granules and regulates their formation. *Front. Plant Sci.* 8:1004. doi: 10.3389/fpls.2017.01004
- Bhosale, R., Boudolf, V., Cuevas, F., Lu, R., Eekhout, T., Hu, Z., et al. (2018). A Spatiotemporal DNA endoploidy map of the *Arabidopsis* root reveals roles for the endocycle in root development and stress adaptation. *Plant Cell* 30, 2330–2351. doi: 10.1105/tpc.17.00983

University of Cologne, and grant from the University of Cologne Centre of Excellence in Plant Sciences to AB-D.

ACKNOWLEDGMENTS

This manuscript has been released as a pre-print at bioRxiv (Westermann et al., 2020). We thank Dr. Marc Jakoby for providing aliquots of the AtKRP, SKL motif, AtNPSN12, AtSYP32, and AtGot1p homolog vectors. We thank Dr. Alexandra Steffens for providing aliquots of the AtDCP1 and AtDCP2 expression vectors. We thank Dr. Lisa Stephan for providing aliquots of the AtMYC1 and AtTTG1 BiFC vectors. We thank Dr. Clement Champion and the research group of Prof. Liam Dolan (University of Oxford) for provision of an aliquot of the PM marker vector MpSYP13a. We thank Dr. Joachim F. Uhrig for donation of pCL112/113 vectors.

SUPPLEMENTARY MATERIAL

The Supplementary Material for this article can be found online at: <https://www.frontiersin.org/articles/10.3389/fpls.2020.569194/full#supplementary-material>

Supplementary Figure 1 | Co-expression of MLRs and MRI with single or triple tags in *Marchantia* epidermal cells. (A,B) Arabidopsis MLRs fused to single fluorescent tag are not expressed. (C,D) The 3xCitrine tag leads MLRs to localize to the cytoplasm. (E) The 3xCitrine tag leads to normal cytosolic and plasma membrane localization of MpMRI. Pictures show maximum projections of z-stack captions (see “Materials and Methods” section for details). Scale bar = 20 μ m.

Supplementary Figure 2 | Bimolecular fluorescent complementation assay quality controls. (A) The functionality of the negative control MpLIP5 was confirmed via co-bombardment of split-versions of MpLIP5 and the *Marchantia* homolog of the known Arabidopsis LIP5 interactor MpSKD1, showing a clear protein interaction in dot-like foci. (B) Split-YFP fusion constructs of AtMYC1 and AtTTG1, known interactors, were co-bombarded and shown to physically interact in *M. polymorpha* thallus epidermal cells, supporting the functionality of AtMYC1-YFP_N. The constructs were co-bombarded with nuclear marker AtKRP1. Scale bar = 20 μ m. Pictures show maximum projections of z-stack captions (see “Materials and Methods” section for details).

Supplementary Figure 3 | Nuclei of *M. polymorpha* cannot be readily stained with DAPI. (A) DAPI staining of Tak-1 epidermal cells of a 4 days-old gemmaling. (B) DAPI staining of leaf epidermal cells of a 2 weeks old *A. thaliana* plant. Note the stained nuclei. All scale bars = 50 μ m.

Supplementary Video 1 | Growing rhizoids stained with propidium iodide.

- Boisson-Dernier, A., Roy, S., Kritsas, K., Grobei, M. A., Jaciubek, M., Schroeder, J. I., et al. (2009). Disruption of the pollen-expressed *FERONIA* homologs *ANXUR1* and *ANXUR2* triggers pollen tube discharge. *Development* 136, 3279–3288. doi: 10.1242/dev.040071
- Boisson-Dernier, A., Franck, C. M., Lituiev, D. S., and Grossniklaus, U. (2015). Receptor-like cytoplasmic kinase MARIS functions downstream of CrRLK1L-dependent signaling during tip growth. *Proc. Natl. Acad. Sci. U.S.A.* 112, 12211–12216. doi: 10.1073/pnas.1512375112
- Bouyer, D., Geier, F., Kragler, F., Schnitger, A., Pesch, M., Wester, K., et al. (2008). Two-dimensional patterning by a trapping/depletion mechanism: the role of TTG1 and GL3 in *Arabidopsis trichome* formation. *PLoS Biol.* 6, e60141. doi: 10.1371/journal.pbio.0060141

- Bowman, J. L., Araki, T., Arteaga-Vazquez, M. A., Berger, F., Dolan, L., Haseloff, J., et al. (2015). The naming of names: guidelines for gene nomenclature in Marchantia. *Plant Cell Physiol.* 57, 257–261.
- Bowman, J. L., Kohchi, T., Yamato, K. T., Jenkins, J., Shu, S., Ishizaki, K., et al. (2017). Insights into land plant evolution garnered from the *Marchantia polymorpha* genome. *Cell* 171, 287–304.
- Bramsiepe, J., Wester, K., Weinl, C., Roodbarkelari, F., Kasili, R., Larkin, J. C., et al. (2010). Endoreplication controls cell fate maintenance. *PLoS Genet.* 6:e1000996. doi: 10.1371/journal.pgen.1000996
- Busch, A., Deckena, M., Almeida-Trapp, M., Kopsischke, S., Kock, C., Schüssler, E., et al. (2019). MpTCP1 controls cell proliferation and redox processes in *Marchantia polymorpha*. *New Phytol.* 224, 1627–1641. doi: 10.1111/nph.16132
- Buschmann, H., Holtmannspötter, M., Borchers, A., O'Donoghue, M. T., and Zachgo, S. (2016). Microtubule dynamics of the centrosome-like polar organizers from the basal land plant *Marchantia polymorpha*. *New Phytol.* 209, 999–1013. doi: 10.1111/nph.13691
- Carella, P., Gogleva, A., Hoey, D. J., Bridgen, A. J., Stolze, S. C., Nakagami, H., et al. (2019). Conserved biochemical defenses underpin host responses to oomycete infection in an early-divergent land plant lineage. *Curr. Biol.* 29, 2282–2294. doi: 10.1016/j.cub.2019.05.078
- Chiyoda, S., Ishizaki, K., Kataoka, H., Yamato, K. T., and Kohchi, T. (2008). Direct transformation of the liverwort *Marchantia polymorpha* L. by particle bombardment using immature thalli developing from spores. *Plant Cell Rep.* 27, 1467–1473. doi: 10.1007/s00299-008-0570-5
- Chiyoda, S., Yamato, K. T., and Kohchi, T. (2014). Plastid transformation of sporelings and suspension-cultured cells from the liverwort *Marchantia polymorpha* L. *Methods Mol. Biol.* 1132, 439–447. doi: 10.1007/978-1-62703-995-6_30
- Conchon, S., Cao, X., Barlowe, C., and Pelham, H. R. B. (1999). Got1p and Sft2p: membrane proteins involved in traffic to the Golgi complex. *EMBO J.* 18, 3934–3946. doi: 10.1093/emboj/18.14.3934
- De Veylder, L., Beeckman, T., Beemster, G. T. S., Krols, L., Terras, F., Landrieu, I., et al. (2001). Functional analysis of cyclin-dependent kinase inhibitors of *Arabidopsis*. *Plant Cell* 13, 1653–1667. doi: 10.1105/tpc.13.7.1653
- Delmans, M., Pollak, B., and Haseloff, J. (2017). MarpoDB: an open registry for *Marchantia polymorpha* genetic parts. *Plant Cell Physiol.* 58:e5. doi: 10.1093/pcp/pcw201
- Eklund, D. M., Kanei, M., Flores-Sandoval, E., Ishizaki, K., Nishihama, R., Kohchi, T., et al. (2018). An evolutionarily conserved abscisic acid signaling pathway regulates dormancy in the liverwort *Marchantia polymorpha*. *Curr. Biol.* 28, 3691–3699. doi: 10.1016/j.cub.2018.10.018
- Feys, B. J., Wiermer, M., Bhat, R. A., Moisan, L. J., Medina-Escobar, N., Neu, C., et al. (2005). *Arabidopsis* SENESCENCE-ASSOCIATED GENE101 stabilizes and signals within an ENHANCED DISEASE SUSCEPTIBILITY1 complex in plant innate immunity. *Plant Cell* 17, 2601–2613. doi: 10.1105/tpc.105.033910
- Flores-Sandoval, E., Eklund, D. M., and Bowman, J. L. (2015). A simple auxin transcriptional response system regulates multiple morphogenetic processes in the liverwort *Marchantia polymorpha*. *PLoS Genet.* 11:e1005207. doi: 10.1371/journal.pgen.1005207
- Franck, C. M., Westermann, J., and Boisson-Dernier, A. (2018a). Plant malectin-like receptor kinases: from cell wall integrity to immunity and beyond. *Ann. Rev. Plant Biol.* 69, 301–328. doi: 10.1146/annurev-arplant-042817-040557
- Franck, C. M., Westermann, J., Bürrsner, S., Lentz, R., Lituiev, D. S., and Boisson-Dernier, A. (2018b). The protein phosphatases ATUNIS1 and ATUNIS2 regulate cell wall integrity in tip-growing cells. *Plant Cell* 30, 1906–1923. doi: 10.1105/tpc.18.00284
- Fukuzawa, H., Kohchi, T., Sano, T., Shirai, H., Umesono, K., Inokuchi, H., et al. (1988). Structure and organization of *Marchantia polymorpha* chloroplast genome: III. Gene organization of the large single copy region from *rbcl* to *trnI* (CAU). *J. Mol. Biol.* 203, 333–351. doi: 10.1016/0022-2836(88)90003-4
- Furuya, T., Hattori, K., Kimori, Y., Ishida, S., Nishihama, R., Kohchi, T., et al. (2018). ANGSTIFOLIA contributes to the regulation of three-dimensional morphogenesis in the liverwort *Marchantia polymorpha*. *Development* 145:dev161398. doi: 10.1242/dev.161398
- Furuya, T., Kimori, Y., and Tsukaya, H. (2019). A method for evaluating three-dimensional morphological features: a case study using *Marchantia polymorpha*. *Front. Plant Sci.* 10:1214. doi: 10.3389/fpls.2019.01214
- Geldner, N., Déneraud-Tendon, V., Hyman, D. L., Mayer, U., Stierhof, Y. D., and Chory, J. (2009). Rapid, combinatorial analysis of membrane compartments in intact plants with a multicolor marker set. *Plant J.* 59, 169–178. doi: 10.1111/j.1365-3113.2009.03851.x
- Gimenez-Ibanez, S., Zamarreño, A. M., García-Mina, J. M., and Solano, R. (2019). An Evolutionarily Ancient Immune System Governs the Interactions between *Pseudomonas syringae* and an early-diverging land plant lineage. *Curr. Biol.* 29, 2270–2281. doi: 10.1016/j.cub.2019.05.079
- Gould, S. J., Keller, G. A., Hosken, N., Wilkinson, J., and Subramani, S. (1989). A conserved tripeptide sorts proteins to peroxisomes. *J. Cell Biol.* 108, 1657–1664. doi: 10.1083/jcb.108.5.1657
- Haas, T. J., Sliwinski, M. K., Martínez, D. E., Preuss, M., Ebine, K., Ueda, T., et al. (2007). The *Arabidopsis* AAA ATPase SKD1 is involved in multivesicular endosome function and interacts with its positive regulator LYST-INTERACTING PROTEIN5. *Plant Cell* 19, 1295–1312. doi: 10.1105/tpc.106.049346
- Hao, L. H., Wang, W. X., Chen, C., Wang, Y. F., Liu, T., Li, X., et al. (2012). Extracellular ATP promotes stomatal opening of *Arabidopsis thaliana* through heterotrimeric G protein α subunit and reactive oxygen species. *Mol. Plant* 5, 852–864. doi: 10.1093/mp/sss095
- Harrison, C. J. (2017). Development and genetics in the evolution of land plant body plans. *Philos. Trans. R. Soc. B Biol. Sci.* 372, 20150490. doi: 10.1098/rstb.2015.0490
- Higo, A., Kawashima, T., Borg, M., Zhao, M., López-Vidriero, I., Sakayama, H., et al. (2018). Transcription factor DUO1 generated by neo-functionalization is associated with evolution of sperm differentiation in plants. *Nat. Commun.* 9, 1–13.
- Hu, C. D., Chinenov, Y., and Kerppola, T. K. (2002). Visualization of interactions among bZIP and Rel family proteins in living cells using bimolecular fluorescence complementation. *Mol. Cell.* 9, 789–798. doi: 10.1016/s1097-2765(02)00496-3
- Ishizaki, K., Chiyoda, S., Yamato, K. T., and Kohchi, T. (2008). Agrobacterium-mediated transformation of the haploid liverwort *Marchantia polymorpha* L., an emerging model for plant biology. *Plant Cell Physiol.* 49, 1084–1091. doi: 10.1093/pcp/pcn085
- Ishizaki, K., Johzuka-Hisatomi, Y., Ishida, S., Iida, S., and Kohchi, T. (2013). Homologous recombination-mediated gene targeting in the liverwort *Marchantia polymorpha* L. *Sci. Rep.* 3, 1–6.
- Ishizaki, K., Nishihama, R., Ueda, M., Inoue, K., Ishida, S., Nishimura, Y., et al. (2015a). Development of gateway binary vector series with four different selection markers for the liverwort *Marchantia polymorpha*. *PLoS One* 10:e0138876. doi: 10.1371/journal.pone.0138876
- Ishizaki, K., Nishihama, R., Yamato, K. T., and Kohchi, T. (2015b). Molecular genetic tools and techniques for *Marchantia polymorpha* research. *Plant Cell Physiol.* 57, 262–270.
- Iwasaki, S., Takeda, A., Motose, H., and Watanabe, Y. (2007). Characterization of *Arabidopsis* decapping proteins AtDCP1 and AtDCP2, which are essential for post-embryonic development. *FEBS Lett.* 581, 2455–2459. doi: 10.1016/j.febslet.2007.04.051
- Jakoby, M. J., Weinl, C., Pusch, S., Kuijt, S. J. H., Merkle, T., Dissmeyer, N., et al. (2006). Analysis of the subcellular localization, function, and proteolytic control of the *Arabidopsis* cyclin-dependent kinase inhibitor ICK1/KRP1. *Plant Physiol.* 141, 1293–1305. doi: 10.1104/pp.106.081406
- Jin, J. P., Zhang, H., Kong, L., Gao, G., and Luo, J. C. (2014). PlantTFDB 3.0: a portal for the functional and evolutionary study of plant transcription factors. *Nucleic Acids Res.* 42, D1182–D1187.
- Jin, J. P., He, K., Tang, X., Li, Z., Lv, L., Zhao, Y., et al. (2015). An *Arabidopsis* transcriptional regulatory map reveals distinct functional and evolutionary features of novel transcription factors. *Mol. Biol. Evol.* 32, 1767–1773. doi: 10.1093/molbev/msv058
- Jin, J. P., Tian, F., Yang, D. C., Meng, Y. Q., Kong, L., Luo, J. C., et al. (2017). PlantTFDB 4.0: toward a central hub for transcription factors and regulatory interactions in plants. *Nucleic Acids Res.* 45, D1040–D1045.
- Jones, K., Kim, D. W., Park, J. S., and Khang, C. H. (2016). Live-cell fluorescence imaging to investigate the dynamics of plant cell death during infection by the rice blast fungus *Magnaporthe oryzae*. *BMC Plant Biol.* 16:69. doi: 10.1186/s12870-016-0756-x

- Jones, V. A., and Dolan, L. (2017). MpWIP regulates air pore complex development in the liverwort *Marchantia polymorpha*. *Development* 144, 1472–1476. doi: 10.1242/dev.144287
- Kanazawa, T., Era, A., Minamino, N., Shikano, Y., Fujimoto, M., Uemura, T., et al. (2016). SNARE molecules in *Marchantia polymorpha*: unique and conserved features of the membrane fusion machinery. *Plant Cell Physiol.* 57, 307–324. doi: 10.1093/pcp/pcv076
- Kato, H., Kouno, M., Takeda, M., Suzuki, H., Ishizaki, K., Nishihama, R., et al. (2017). The roles of the sole activator-type auxin response factor in pattern formation of *Marchantia polymorpha*. *Plant Cell Physiol.* 58, 1642–1651. doi: 10.1093/pcp/pcx095
- Keller, G. A., Krisans, S., Gould, S. J., Sommer, J. M., Wang, C. C., Schliebs, W., et al. (1991). Evolutionary conservation of a microbody targeting signal that targets proteins to peroxisomes, glyoxysomes, and glycosomes. *J. Cell Biol.* 114, 893–904. doi: 10.1083/jcb.114.5.893
- Kim, J., Lee, H., Lee, H. N., Kim, S. H., Shin, K. D., and Chung, T. (2013). Autophagy-related proteins are required for degradation of peroxisomes in *Arabidopsis* hypocotyls during seedling growth. *Plant Cell* 25, 4956–4966. doi: 10.1105/tpc.113.117960
- Kimura, S., and Kodama, Y. (2016). Actin-dependence of the chloroplast cold positioning response in the liverwort *Marchantia polymorpha* L. *PeerJ* 4:e2513. doi: 10.7717/peerj.2513
- Kirchhelle, C., Chow, C. M., Foucart, C., Neto, H., Stierhof, Y. D., Kalde, M., et al. (2016). The Specification of Geometric Edges by a Plant Rab GTPase is an essential cell-patterning principle during organogenesis in *Arabidopsis*. *Dev. Cell* 36, 386–400. doi: 10.1016/j.devcel.2016.01.020
- Kirik, V., Bouyer, D., Schöbinger, U., Bechtold, N., Herzog, M., Bonneville, J. M., et al. (2001). CPR5 is involved in cell proliferation and cell death control and encodes a novel transmembrane protein. *Curr. Biol.* 11, 1891–1895. doi: 10.1016/s0960-9822(01)00590-5
- Kodama, Y., and Hu, C. D. (2012). Bimolecular fluorescence complementation (BiFC): a 5-year update and future perspectives. *Biotechniques* 53, 285–298.
- Kohchi, T., Shirai, H., Fukuzawa, H., Sano, T., Komano, T., Umesono, K., et al. (1988). Structure and organization of *Marchantia polymorpha* chloroplast genome: IV. Inverted repeat and small single copy regions. *J. Mol. Biol.* 203, 353–372. doi: 10.1016/0022-2836(88)90004-6
- Kondou, Y., Miyagi, Y., Morito, T., Fujihira, K., Miyauchi, W., Moriyama, A., et al. (2019). Physiological function of photoreceptor UVR8 in UV-B tolerance in the liverwort *Marchantia polymorpha*. *Planta* 249, 1349–1364. doi: 10.1007/s00425-019-03090-w
- Kong, X., Li, C., Zhang, F., Yu, Q., Gao, S., Zhang, M., et al. (2018). Ethylene promotes cadmium-induced root growth inhibition through EIN3 controlled XTH33 and LSU1 expression in *Arabidopsis*. *Plant Cell Environ.* 41, 2449–2462. doi: 10.1111/pce.13361
- Konno, R., Tanaka, H., and Kodama, Y. (2018). SKLPT imaging: efficient in vivo pre-evaluation of genome-editing modules using fluorescent protein with peroxisome targeting signal. *Biochem. Biophys. Res. Commun.* 503, 235–241. doi: 10.1016/j.bbrc.2018.06.008
- Kost, B., Spielhofer, P., and Chua, N. H. (1998). A GFP-mouse talin fusion protein labels plant actin filaments in vivo and visualizes the actin cytoskeleton in growing pollen tubes. *Plant J.* 16, 393–401. doi: 10.1046/j.1365-313x.1998.00304.x
- Kubota, A., Ishizaki, K., Hosaka, M., and Kohchi, T. (2013). Efficient Agrobacterium-mediated transformation of the liverwort *Marchantia polymorpha* using regenerating thalli. *Biosci. Biotechnol. Biochem.* 77, 167–172.
- Lee, Y. K., Kim, G. T., Kim, I. J., Park, J., Kwak, S. S., Choi, G., et al. (2006). LONGIFOLIA1 and LONGIFOLIA2, two homologous genes, regulate longitudinal cell elongation in *Arabidopsis*. *Development* 133, 4305–4314. doi: 10.1242/dev.02604
- Lind, C., Dreyer, I., López-Sanjurjo, E. J., von Meyer, K., Ishizaki, K., Kohchi, T., et al. (2015). Stomatal guard cells co-opted an ancient ABA-dependent desiccation survival system to regulate stomatal closure. *Curr. Biol.* 25, 928–935. doi: 10.1016/j.cub.2015.01.067
- Maldonado-Bonilla, L. D. (2014). Composition and function of P bodies in *Arabidopsis thaliana*. *Front. Plant Sci.* 5:201. doi: 10.3389/fpls.2014.00201
- Mang, H., Feng, B., Hu, Z., Boisson-Dernier, A., Franck, C. M., Meng, X., et al. (2017). Differential regulation of two-tiered plant immunity and sexual reproduction by ANXUR receptor-like kinases. *Plant Cell* 29, 3140–3156. doi: 10.1105/tpc.17.00464
- Mano, S., Nishihama, R., Ishida, S., Hikino, K., Kondo, M., Nishimura, M., et al. (2018). Novel gateway binary vectors for rapid tripartite DNA assembly and promoter analysis with various reporters and tags in the liverwort *Marchantia polymorpha*. *PLoS One* 13:e0204964. doi: 10.1371/journal.pone.0204964
- Mathur, J., Mathur, N., and Hülskamp, M. (2002). Simultaneous visualization of peroxisomes and cytoskeletal elements reveals actin and not microtubule-based peroxisome motility in plants. *Plant Physiol.* 128, 1031–1045. doi: 10.1104/pp.011018
- Mathur, J., Mathur, N., Kernebeck, B., and Hülskamp, M. (2003). Mutations in Actin-related proteins 2 and 3 affect Cell Shape Development in *Arabidopsis*. *Plant Cell* 15, 1632–1645. doi: 10.1105/tpc.011676
- Minamino, N., Kanazawa, T., Era, A., Ebine, K., Nakano, A., and Ueda, T. (2018). RAB GTPases in the Basal Land Plant *Marchantia polymorpha*. *Plant Cell Physiol.* 59, 845–856.
- Miyazaki, S., Murata, T., Sakurai-Ozato, N., Kubo, M., Demura, T., Fukuda, H., et al. (2009). ANXUR1 and 2, sister genes to FERONIA/SIRENE, are male factors for coordinated fertilization. *Curr. Biol.* 19, 1327–1331. doi: 10.1016/j.cub.2009.06.064
- Monte, I., Franco-Zorrilla, J. M., García-Casado, G., Zamarreño, A. M., García-Mina, J. M., Nishihama, R., et al. (2019). A single JAZ repressor controls the jasmonate pathway in *Marchantia polymorpha*. *Mol. plant* 12, 185–198. doi: 10.1016/j.molp.2018.12.017
- Monte, I., Ishida, S., Zamarreño, A. M., Hamberg, M., Franco-Zorrilla, J. M., García-Casado, G., et al. (2018). Ligand-receptor co-evolution shaped the jasmonate pathway in land plants. *Nature chem. Biol.* 14:480. doi: 10.1038/s41589-018-0033-4
- Morris, J. L., Puttick, M. N., Clark, J. W., Edwards, D., Kenrick, P., Pressel, S., et al. (2018). The timescale of early land plant evolution. *Proc. Natl. Acad. Sc. U.S.A.* 115, E2274–E2283.
- Motomura, K., Le, Q. T. N., Hamada, T., Kutsuna, N., Mano, S., Nishimura, M., et al. (2015). Diffuse decapping enzyme DCP2 accumulates in DCP1 foci under heat stress in *Arabidopsis thaliana*. *Plant Cell Physiol.* 56, 107–115. doi: 10.1093/pcp/pcu151
- Nagai, J. I., Yamato, K. T., Sakaida, M., Yoda, H., Fukuzawa, H., Ohyama, K., et al. (1999). Expressed sequence tags from immature female sexual organ of a liverwort, *Marchantia polymorpha*. *DNA Res.* 6, 1–11. doi: 10.1093/dnares/6.1.1
- Naito, Y., Hino, K., Bono, H., and Ui-Tei, K. (2015). CRISPRdirect: software for designing CRISPR/Cas guide RNA with reduced off-target sites. *Bioinformatics* 31, 1120–1123. doi: 10.1093/bioinformatics/btu743
- Nishiyama, R., Yamato, K. T., Miura, K., Sakaida, M., Okada, S., Kono, K., et al. (2000). Comparison of expressed sequence tags from male and female sexual organs of *Marchantia polymorpha*. *DNA Res.* 7, 165–174. doi: 10.1093/dnares/7.3.165
- Ohyama, K., Fukuzawa, H., Kohchi, T., Sano, T., Sano, S., Shirai, H., et al. (1988). Structure and organization of *Marchantia polymorpha* chloroplast genome: I. Cloning and gene identification. *J. Mol. Biol.* 203, 281–298. doi: 10.1016/0022-2836(88)90001-0
- Otani, K., Ishizaki, K., Nishihama, R., Takatani, S., Kohchi, T., Takahashi, T., et al. (2018). An evolutionarily conserved NIMA-related kinase directs rhizoid tip growth in the basal land plant *Marchantia polymorpha*. *Development* 145:dev154617. doi: 10.1242/dev.154617
- Peñuelas, M., Monte, I., Schweizer, F., Vallat, A., Reymond, P., García-Casado, G., et al. (2019). Jasmonate-related MYC Transcription Factors are Functionally Conserved in *Marchantia polymorpha*. *Plant Cell* 31, 2491–2509. doi: 10.1105/tpc.18.00974
- Pesch, M., Schultheiß, I., Digiuni, S., Uhrig, J. F., and Hülskamp, M. (2013). Mutual control of intracellular localisation of the patterning proteins ATMYC1, GL1 and TRY/CPC in *Arabidopsis*. *Development* 140, 3456–3467. doi: 10.1242/dev.094698
- Proust, H., Honkanen, S., Jones, V. A., Morieri, G., Prescott, H., Kelly, S., et al. (2016). RSL class I genes controlled the development of epidermal structures in the common ancestor of land plants. *Curr. Biol.* 26, 93–99.
- Puttick, M. N., O'Reilly, J. E., Tanner, A. R., Fleming, J. F., Clark, J., Holloway, L., et al. (2017). Uncertain-tree: discriminating among competing approaches to the phylogenetic analysis of phenotype data. *Proc. R. Soc. B Biol. Sci.* 284:20162290. doi: 10.1098/rspb.2016.2290

- Rasmussen, J. L., Kikkert, J. R., Roy, M. K., and Sanford, J. C. (1994). Biolistic transformation of tobacco and maize suspension cells using bacterial cells as microprojectiles. *Plant Cell Rep.* 13, 212–217.
- Riedl, J., Crevenna, A. H., Kessenbrock, K., Yu, J. H., Neukirchen, D., Bista, M., et al. (2008). Lifeact: a versatile marker to visualize F-actin. *Nat. Methods* 5, 605–607. doi: 10.1038/nmeth.1220
- Rodríguez-Serrano, M., Romero-Puertas, M. C., Sanz-Fernández, M., Hu, J., and Sandalio, L. M. (2016). Peroxisomes extend peroxules in a fast response to stress via a reactive oxygen species-mediated induction of the peroxin PEX11a. *Plant Physiol.* 171, 1665–1674. doi: 10.1104/pp.16.00648
- Rotman, B., and Papermaster, B. W. (1966). Membrane properties of living mammalian cells as studied by enzymatic hydrolysis of fluorogenic esters. *PNAS* 55, 134–141. doi: 10.1073/pnas.55.1.134
- Rövekamp, M., Bowman, J. L., and Grossniklaus, U. (2016). Marchantia MpRKD regulates the gametophyte-sporophyte transition by keeping egg cells quiescent in the absence of fertilization. *Curr. Biol.* 26, 1782–1789. doi: 10.1016/j.cub.2016.05.028
- Saedler, R., Jakoby, M., Marin, B., Galiana-jaime, E., and Hu, M. (2009). The cell morphogenesis gene SPIRRIG in *Arabidopsis* encodes a WD / BEACH domain protein. *Plant J.* 59, 612–621. doi: 10.1111/j.1365-313x.2009.03900.x
- Sanford, J. C. (1990). Biolistic plant transformation. *Phys. Plant.* 79, 206–209. doi: 10.1034/j.1399-3054.1990.790131.x
- Sato, Y., Sugimoto, N., Hirai, T., Imai, A., Kubo, M., Hiwatashi, Y., et al. (2017). Cells reprogramming to stem cells inhibit the reprogramming of adjacent cells in the moss *Physcomitrella patens*. *Sci. Rep.* 7, 1–12.
- Sauret-Güeto, S., Frangedakis, E., Silvestri, L., Rebmann, M., Tomaselli, M., Markel, K., et al. (2020). Systematic tools for reprogramming plant gene expression in a simple model, *Marchantia polymorpha*. *ACS Synthetic Biol.* 9, 864–882. doi: 10.1021/acssynbio.9b00511
- Schapiro, A. L., Voigt, B., Jasik, J., Rosado, A., Lopez-Cobollo, R., Menzel, D., et al. (2008). *Arabidopsis* Synaptotagmin 1 is required for the maintenance of plasma membrane integrity and cell viability. *Plant Cell* 20, 3374–3388. doi: 10.1105/tpc.108.063859
- Schindelin, J., Arganda-Carreras, I., Frise, E., Kaynig, V., Longair, M., Pietzsch, T., et al. (2012). Fiji: an open-source platform for biological-image analysis. *Nat. Methods* 9, 676–682. doi: 10.1038/nmeth.2019
- Schnittger, A., and Hülskamp, M. (2007). Whole-Mount DAPI staining and measurement of DNA content in plant cells. *CSH Protoc.* 2007.pdb.prot4684. doi: 10.1101/pdb.prot4684
- Schnittger, A., Weinel, C., Bouyer, D., Schöbinger, U., and Hülskamp, M. (2003). Misexpression of the cyclin-dependent kinase inhibitor ICK1/KRP1 in single-celled *Arabidopsis trichomes* reduces endoreduplication and cell size and induces cell death. *Plant Cell* 15, 303–315. doi: 10.1105/tpc.008342
- Shahriari, M., Keshavaiah, C., Scheuring, D., Sabovljevic, A., Pimpl, P., Häusler, R. E., et al. (2010). The AAA-type ATPase AtSKD1 contributes to vacuolar maintenance of *Arabidopsis thaliana*. *Plant J.* 64, 71–85.
- Sharma, N., Jung, C. H., Bhalla, P. L., and Singh, M. B. (2014). RNA sequencing analysis of the gametophyte transcriptome from the liverwort, *Marchantia polymorpha*. *PLoS One* 9:e97497. doi: 10.1371/journal.pone.0097497
- Shaw, A. J., Szövényi, P., and Shaw, B. (2011). Bryophyte diversity and evolution: windows into the early evolution of land plants. *Am. J. Bot.* 98, 352–369. doi: 10.3732/ajb.1000316
- Spitzer, C., Schellmann, S., Sabovljevic, A., Shahriari, M., Keshavaiah, C., Bechtold, N., et al. (2006). The *Arabidopsis elch* mutant reveals functions of an ESCRT components in cytokinesis. *Development* 133, 4679–4689. doi: 10.1242/dev.02654
- Steffens, A., Bräutigam, A., Jakoby, M., and Hülskamp, M. (2015). The BEACH Domain Protein SPIRRIG is essential for *Arabidopsis* salt stress tolerance and functions as a regulator of transcript stabilization and localization. *PLoS Biol.* 13:e1002188. doi: 10.1371/journal.pbio.1002188
- Steffens, A., Jaegle, B., Tresch, A., Hülskamp, M., and Jakoby, M. (2014). Processing-Body Movement in *Arabidopsis* depends on an interaction between Myosins and DECAPPING PROTEIN1. *Plant Physiol.* 164, 1879–1892. doi: 10.1104/pp.113.233031
- Steffens, A., Jakoby, M., and Hülskamp, M. (2017). Physical, Functional and Genetic Interactions between the BEACH Domain Protein SPIRRIG and LIP5 and SKD1 and Its Role in Endosomal Trafficking to the Vacuole in *Arabidopsis*. *Front. Plant Sci.* 8:1969. doi: 10.3389/fpls.2017.01969
- Sugano, S. S., and Nishiyama, R. (2018). CRISPR/Cas9-Based Genome Editing of Transcription Factor Genes in *Marchantia polymorpha*. *Methods Mol. Biol.* 1830, 109–126. doi: 10.1007/978-1-4939-8657-6_7
- Sugano, S. S., Shirakawa, M., Takagi, J., Matsuda, Y., Shimada, T., Hara-Nishimura, L., et al. (2014). CRISPR/Cas9-mediated targeted mutagenesis in the liverwort *Marchantia polymorpha* L. *Plant Cell Physiol.* 55, 475–481. doi: 10.1093/pcp/pcu014
- Sugawara, Y., and Fukukawa, E. (1995). Protoplasts of *Marchantia polymorpha* are stabilized by low concentrations of cellulase in the medium during the early stage of culture. *Plant Tissue Cult. Lett.* 12, 179–185. doi: 10.5511/plantbiotechnology1984.12.179
- Takano, J., Noguchi, K., Yasumori, M., Kobayashi, M., Gajdos, Z., Miwa, K., et al. (2002). *Arabidopsis* boron transporter for xylem loading. *Nature* 420, 337–340. doi: 10.1038/nature01139
- Takenaka, M., Yamaoka, S., Hanajiri, T., Shimizu-Ueda, Y., Yamato, K. T., Fukuzawa, H., et al. (2000). Direct transformation and plant regeneration of the haploid liverwort *Marchantia polymorpha* L. *Transgenic Res.* 9, 179–185.
- Thamm, A., Saunders, T. E., and Dolan, L. (2020). MpFEW RHIZOIDS1 miRNA-mediated lateral inhibition controls rhizoid cell patterning in *Marchantia polymorpha*. *Curr. Biol.* 30, 1905–1915. doi: 10.1016/j.cub.2020.03.032
- Ubeda-Tomás, S., Federici, F., Casimiro, I., Beemster, G. T. S., Bhalerao, R., Swarup, R., et al. (2009). Gibberellin signaling in the endodermis controls *arabidopsis* root meristem size. *Curr. Biol.* 19, 1194–1199. doi: 10.1016/j.cub.2009.06.023
- Ueki, S., Lacroix, B., Krichevsky, A., Lazarowitz, S. G., and Citovsky, V. (2009). Functional native genetic transformation of *Arabidopsis* leaves by biolistic bombardment. *Nat. Protoc.* 4, 71–77. doi: 10.1038/nprot.2008.217
- Uemura, T., Ueda, T., Ohniwa, R. L., Nakano, A., Takeyasu, K., and Sato, M. H. (2004). Systematic analysis of SNARE molecules in *Arabidopsis*: dissection of the post-Golgi network in plant cells. *Cell Struct. Funct.* 29, 49–65. doi: 10.1247/csf.29.49
- Umesono, K., Inokuchi, H., Shiki, Y., Takeuchi, M., Chang, Z., Fukuzawa, H., et al. (1988). Structure and organization of *Marchantia polymorpha* chloroplast genome: II. Gene organization of the large single copy region from *rps* 12 to *atpB*. *J. Mol. Biol.* 203, 299–331. doi: 10.1016/0022-2836(88)90002-2
- Walter, M., Chaban, C., Schütze, K., Batistic, O., Weckermann, K., Näge, C., et al. (2004). Visualization of protein interactions in living plant cells using bimolecular fluorescence complementation. *Plant J.* 40, 428–438.
- Wang, H., Qi, Q., Schorr, P., Cutler, A. J., Crosby, W. L., and Fowke, L. C. (1998). ICK1, a cyclin-dependent protein kinase inhibitor from *Arabidopsis thaliana* interacts with both Cdc2a and CycD3, and its expression is induced by abscisic acid. *Plant J.* 15, 501–510. doi: 10.1046/j.1365-313x.1998.00231.x
- Weber, C., Nover, L., and Fauth, M. (2008). Plant stress granules and mRNA processing bodies are distinct from heat stress granules. *Plant J.* 56, 517–530. doi: 10.1111/j.1365-313x.2008.03623.x
- Weinel, C., Marquardt, S., Kuijt, S. J. H., Nowack, M. K., Jakoby, M. J., Hülskamp, M., et al. (2005). Novel functions of plant cyclin-dependent kinase inhibitors, ICK1/KRP1, can act non-cell-autonomously and inhibit entry into mitosis. *Plant Cell* 17, 1704–1722. doi: 10.1105/tpc.104.030486
- Westermann, J., Koebke, E., Lentz, R., Hülskamp, M., and Boisson-Dernier, A. (2020). A comprehensive toolkit for quick and easy visualization of marker proteins, protein-protein interactions and cell morphology in *Marchantia polymorpha*. *bioRxiv [Preprint]* doi: 10.1101/2020.04.20.050054
- Westermann, J., Streubel, S., Franck, C. M., Lentz, R., Dolan, L., and Boisson-Dernier, A. (2019). An evolutionarily conserved receptor-like kinases signaling module controls cell wall integrity during tip growth. *Curr. Biol.* 29, 3899–3908. doi: 10.1016/j.cub.2019.09.069
- Xu, J., and Chua, N. H. (2009). *Arabidopsis* decapping 5 is required for mRNA decapping, P-body formation, and translational repression during postembryonic development. *Plant Cell* 21, 3270–3279. doi: 10.1105/tpc.109.070078
- Xu, J., Yang, J. Y., Niu, Q. W., and Chua, N. H. (2006). *Arabidopsis* DCP2, DCP1, and VARICOSE form a decapping complex required for

- postembryonic development. *Plant Cell* 18, 3386–3398. doi: 10.1105/tpc.106.047605
- Zhao, H., Wang, X., Zhu, D., Cui, S., Li, X., Cao, Y., et al. (2012). A single amino acid substitution in IIIf subfamily of basic helix-loop-helix transcription factor AtMYC1 leads to trichome and root hair patterning defects by abolishing its interaction with partner proteins in *Arabidopsis*. *J. Biol. Chem.* 287, 14109–14121. doi: 10.1074/jbc.m111.280735
- Zimmermann, I. M., Heim, M. A., Weisshaar, B., and Uhrig, J. F. (2004). Comprehensive identification of *Arabidopsis thaliana* MYB transcription factors interacting with R/B-like BHLH proteins. *Plant J.* 40, 22–34. doi: 10.1111/j.1365-313x.2004.02183.x
- Conflict of Interest:** The authors declare that the research was conducted in the absence of any commercial or financial relationships that could be construed as a potential conflict of interest.

Copyright © 2020 Westermann, Koebke, Lentz, Hülskamp and Boisson-Dernier. This is an open-access article distributed under the terms of the Creative Commons Attribution License (CC BY). The use, distribution or reproduction in other forums is permitted, provided the original author(s) and the copyright owner(s) are credited and that the original publication in this journal is cited, in accordance with accepted academic practice. No use, distribution or reproduction is permitted which does not comply with these terms.